

Experimental and Theoretical Study on the Role of Monomeric vs Dimeric Rhodium Oxazolidinone Norbornadiene Complexes in Catalytic Asymmetric 1,2- and 1,4-Additions

Manuel Kirchhof, Katrin Gugeler, Felix Richard Fischer, Michal Nowakowski, Alina Bauer, Sonia Alvarez-Barcia, Karina Abitaev, Marc Schnierle, Yaseen Qawasmi, Wolfgang Frey, Angelika Baro, Deven P. Estes, Thomas Sottmann,* Mark R. Ringenberg,* Bernd Plietker,* Matthias Bauer,* Johannes Kästner,* and Sabine Laschat*

Cite This: <https://dx.doi.org/10.1021/acs.organomet.0c00310>

Read Online

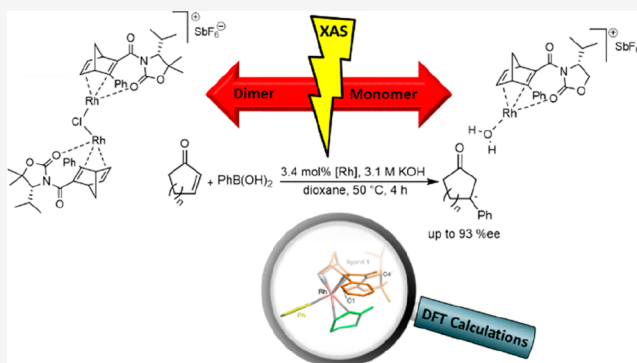
ACCESS |

Metrics & More

Article Recommendations

Supporting Information

ABSTRACT: The influence of nuclearity and charge of chiral Rh diene complexes on the activity and enantioselectivity in catalytic asymmetric 1,2-additions of organoboron reagents to *N*-tosylimines and 1,4-additions to enones was investigated. For this purpose, cationic dimeric Rh(I) complex $[(\text{Rh}(\text{1}))_2\text{Cl}]\text{SbF}_6$ and cationic monomeric Rh(I) complex $[\text{RhOH}_2(\text{2})]\text{SbF}_6$ were synthesized from oxazolidinone-substituted 3-phenylnorbornadiene ligands **1** and **2**, which differ in the substitution pattern at oxazolidinone C-5' (CMe_2 vs CH_2) and compared with the corresponding neutral dimeric and monomeric Rh(I) complexes $[\text{RhCl}(\text{1})]_2$ and $[\text{RhCl}(\text{2})]$. Structural, electronic, and mechanistic insights were gained by X-ray crystallography, cyclic voltammetry (CV), X-ray absorption spectroscopy (XAS), and DFT calculations. CV revealed an increased stability of cationic vs neutral Rh complexes toward oxidation. Comparison of solid-state and solution XAS (extended X-ray absorption fine structure (EXAFS), X-ray absorption near edge structure (XANES)) data showed that the monomeric Rh complex $[\text{RhCl}(\text{2})]$ maintained its electronic state and coordination sphere in solution, whereas the dimeric Rh complex $[\text{RhCl}(\text{1})]_2$ exchanges bridging chloro ligands by dioxane molecules in solution. In both 1,2- and 1,4-addition reactions, monomeric Rh complexes $[\text{RhCl}(\text{2})]$ and $[\text{RhOH}_2(\text{2})]\text{SbF}_6$ gave better yields as compared to dimeric complexes $[\text{RhCl}(\text{1})]_2$ and $[(\text{Rh}(\text{1}))_2\text{Cl}]\text{SbF}_6$. Regarding enantioselectivities, dimeric Rh species $[\text{RhCl}(\text{1})]_2$ and $[(\text{Rh}(\text{1}))_2\text{Cl}]\text{SbF}_6$ performed better than monomeric Rh species in the 1,2-addition, while the opposite was true for the 1,4-addition. Neutral Rh complexes performed better than cationic complexes. Microemulsions improved the yields of 1,2-additions due to a most probable enrichment of Rh complexes in the amphiphilic film and provided a strong influence of the complex nuclearity and charge on the stereocontrol. A strong nonlinear-like effect (NLE) was observed in 1,2-additions, when diastereomeric mixtures of ligands **1** and *epi-1* were employed. The pronounced substrate dependency of the 1,4-addition could be rationalized by DFT calculations.

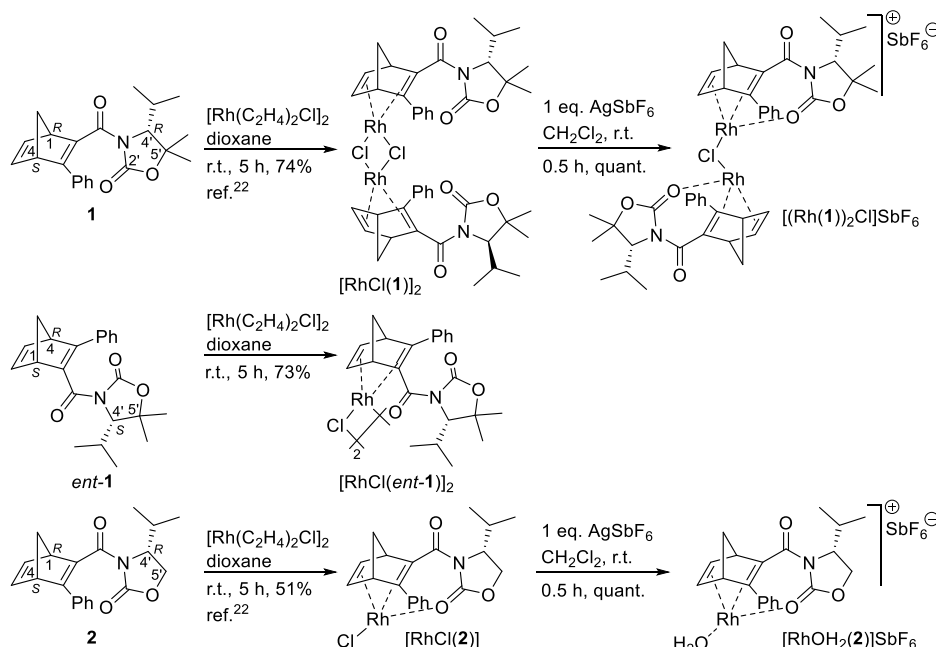


INTRODUCTION

The pioneering discovery by Hayashi, Carreira, and Grützmacher that chiral alkene and diene ligands enable efficient stereocontrol in asymmetric catalysis has delivered highly attractive alternatives to well-known chiral phosphorus and nitrogen ligands.^{1–4} A large variety of chiral diene ligands has been developed since then.^{4,5} The scope of Rh-, Ir-, or Pd-catalyzed reactions has then expanded from 1,2- and 1,4-additions at electron-poor double bonds⁶ to reductions,⁷ cycloadditions,⁸ isomerizations, rearrangements,⁹ and carbene insertions into B–H bonds¹⁰ among others.¹¹ As far as Rh (and Ir) catalysis are concerned, the majority of studies has dealt with dinuclear catalyst precursors $[\text{Rh}(\text{diene}^*)\text{Cl}]_2$ or $[(\text{Ir}(\text{diene}^*)\text{Cl})_2]$, while less work has been carried out with

mononuclear Rh complexes. Dimerization of the $\text{Rh}(\text{diene}^*)\text{X}$ fragment has either been suppressed by the use of monophosphines,¹² chelating diphosphines such as BINAP (2,2'-bis(diphenylphosphino)-1,1'-binaphthyl) or MeO-BIPHEP (2,2'-bis(diphenylphosphino)-6,6'-dimethoxy-1,1'-biphenyl),^{7,13} TADDOL ($\alpha,\alpha',\alpha',\alpha'$ -tetraaryl-1,3-dioxolan-4,5-dimethanol)-derived cyclic monophosphonites,¹⁴ or η^6 -bound

Received: May 4, 2020

Scheme 1. Synthesis of Dimeric and Monomeric Rhodium Complexes^a

^aNeutral Rh(I) complexes $[\text{RhCl}(\mathbf{1})]_2$ and $[\text{RhCl}(\mathbf{2})]$ were prepared according to ref 22 and used for comparison and as precursors for the corresponding cationic Rh(I) complexes.

tetraphenylborates¹⁵ and binaphthylidiamines.¹⁶ Alternatively, tridentate chiral diene–phosphine ligands have been employed, where the phosphine moiety is tethered via an electron-deficient alkene to the diene, resulting in a chelating coordination mode that stabilizes the active cationic Rh(I) catalyst.¹⁷

Moreover, despite the plethora of known chiral diene ligands and their use in Rh(I) catalysis, the majority of studies focused on ligand design, catalytic reactions, and subsequent synthetic applications.⁴ The preparative work was complemented by a small number of reports on nonlinear effects (NLE),¹⁸ kinetic studies,^{19,21} NMR experiments,^{18,20} as well as a series of theoretical investigations.²¹ Most surprisingly, neither X-ray absorption spectroscopy (XAS) (to obtain information on the coordination sphere around rhodium via extended X-ray absorption fine structure (EXAFS) and information on the electronic configuration and orbitals of Rh via X-ray absorption near edge structure (XANES)) nor electrochemical experiments (to get insight into the redox behavior of the Rh complexes) have been carried out. Such information will be helpful in the design of Rh(diene*) catalysts and the suppression of side reactions.

Recently, we developed novel Rh norbornadiene oxazolidinone complexes for catalysis in liquid confinement provided by nanostructured microemulsions.²² We found that, when employing slightly polar and diastereomerically pure norbornadiene oxazolidinone ligands, the catalytic reactions were sluggish in dioxane and almost ceased in toluene, while microemulsions markedly improved the conversion and enantioselectivity as well as reaction rate.

Serendipity helped us to obtain X-ray crystal structures from the neutral dinuclear complex $[\text{RhCl}(\mathbf{1})]_2$ carrying two additional methyl groups at C-5' of the oxazolidinone moiety as well as the neutral mononuclear complex $[\text{RhCl}(\mathbf{2})]$ with H atoms instead of geminal-dimethyl at C-5' (Scheme 1). Catalytic 1,2-additions suggested that both catalysts not only differ in their solid-state structure but seem to have different reactivity and

enantioselectivity. Thus, we decided to investigate the performance of monomeric and dimeric Rh complexes as well as cationic complexes with respect to asymmetric 1,2- and 1,4-additions in more detail using both dioxane and microemulsions as reaction media. In the current manuscript, we report for the first time an assessment of the catalytic performance of a series of structurally similar Rh complexes, which differ in their aggregation state and nuclearity (mono- vs dinuclear and neutral vs cationic). These complexes have been investigated by X-ray crystal structure analysis, cyclic voltammetry, XAS, and computational methods.

RESULTS AND DISCUSSION

Synthesis and Solid-State Structures of Rh Complexes.

The synthesis of the complexes is shown in Scheme 1. Diene ligands of known (1*R*,4*S*,4'*R*)-configuration **1** and **2**²² were treated with the commercially available Rh precursor complex $[\text{Rh}(\text{C}_2\text{H}_4)_2\text{Cl}]_2$ in dioxane for 5 h at room temperature, and the resulting solids were purified by recrystallization to give a 74% yield of dimeric $[\text{RhCl}(\mathbf{1})]_2$ as deep red needles and 51% of monomeric $[\text{RhCl}(\mathbf{2})]$ as yellow needles, respectively. Both complexes were dissolved in CH_2Cl_2 and treated with 1 equiv of AgSbF_6 at room temperature for 0.5 h. After workup, both the cationic dinuclear complex $[(\text{Rh}(\mathbf{1}))_2\text{Cl}]\text{SbF}_6$ and the cationic mononuclear complex $[\text{RhOH}_2(\mathbf{2})]\text{SbF}_6$ were isolated in quantitative yield as yellow solids. In addition, the optical antipode of known (1*R*,4*S*,4'*R*)-configured ligand **1**, i.e., the (1*S*,4*R*,4'*S*)-configured ligand *ent*-**1**, was treated with the Rh precursor complex as described above, and the resulting dimeric neutral complex $[\text{RhCl}(\textit{ent}\text{-}\mathbf{1})]_2$ was obtained in 73% as red needles.

Crystals of the three Rh complexes suitable for single crystal X-ray structure analysis were obtained by recrystallization from Et_2O ($[\text{RhCl}(\textit{ent}\text{-}\mathbf{1})]_2$) or by crystallization in the cold ($[(\text{RhOH}_2(\mathbf{2}))]\text{SbF}_6$ and $[(\text{Rh}(\mathbf{1}))_2\text{Cl}]\text{SbF}_6$) (Figures 1 and S2 and Tables S5 and S6). Relevant geometric data are summarized

in Table 1 and compared with known crystal structures of $[\text{RhCl}(\mathbf{1})]_2$ and $[\text{RhCl}(\mathbf{2})]$.²²

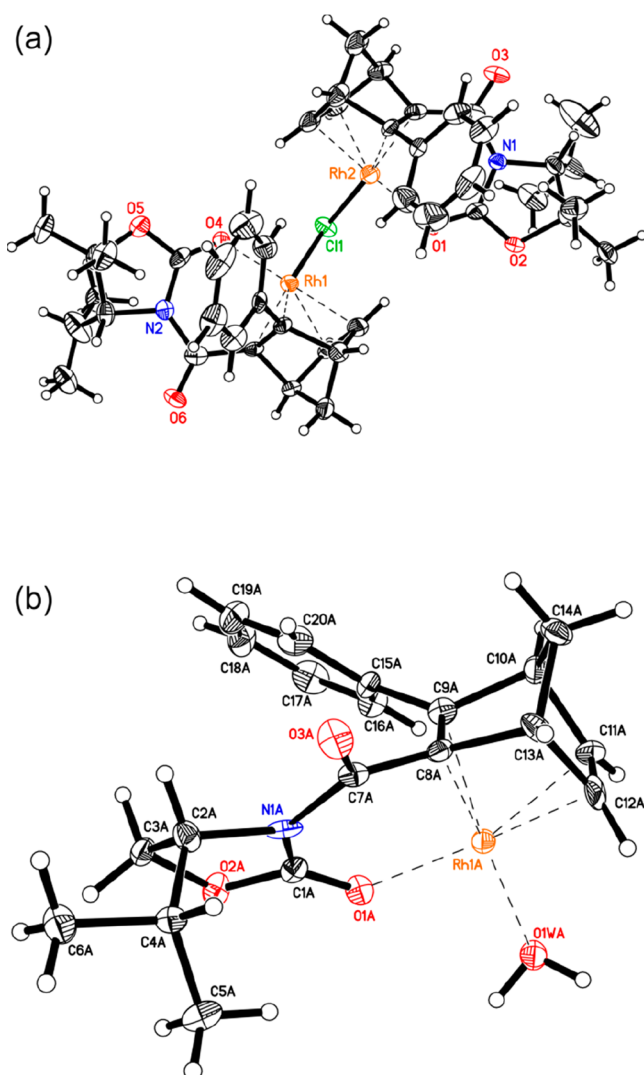


Figure 1. Solid-state structures of (a) cationic dimeric Rh complex $[(\text{Rh}(\mathbf{1}))_2\text{Cl}]\text{SbF}_6$ and (b) cationic monomeric complex $[\text{RhOH}_2(\mathbf{2})]\text{SbF}_6$ (only one of the two conformers is shown). Both complexes possess the (1*R*,4*S*,4'*R*)-configuration. Selected bond distances and angles are listed in Table 1. For getting better overall standard deviations of the geometric parameters of the $[(\text{Rh}(\mathbf{1}))_2\text{Cl}]\text{SbF}_6$ and $[\text{RhOH}_2(\mathbf{2})]\text{SbF}_6$ X-ray structures, a severely disordered Et_2O solvate molecule was removed with SQUEEZE as implemented in PLATON.²³

The cationic monomeric complex $[\text{RhOH}_2(\mathbf{2})]\text{SbF}_6$ crystallized with two conformer ion pairs in the asymmetric unit. The norbornadiene double bonds, the oxazolidinone carbonyl oxygen ($\text{C}=\text{O}$), and one water molecule coordinate to the rhodium center (Figure 1b and Table 1). The cationic dimeric complex $[(\text{Rh}(\mathbf{1}))_2\text{Cl}]\text{SbF}_6$ crystallized with one ion pair in the asymmetric unit. The cationic complex forms dimers, where one μ -chloro bridge connects both Rh centers. They both coordinate the norbornadiene double bonds and the oxazolidinone carbonyl functions (Figure 1a). The neutral dimeric complex $[\text{RhCl}(\text{ent-1})]_2$ ligated by *ent-1* crystallized as one neutral complex in the asymmetric unit (Figure S2 and Table S6). In agreement with previous results²² interactions of the norborna-

diene double bonds with Rh elongate the $\text{C}=\text{C}$ bond lengths in comparison to free ligand (1*S*,4*R*,4'*S*)-1.

The X-ray crystal structure data of all Rh complexes shown in Scheme 1 enabled the determination of unique structural features for each complex and identification of differences within the series. Comparison of the cationic dimer $[(\text{Rh}(\mathbf{1}))_2\text{Cl}]\text{SbF}_6$ and cationic monomer $[\text{RhOH}_2(\mathbf{2})]\text{SbF}_6$ with the corresponding neutral complexes $[\text{RhCl}(\mathbf{1})]_2$,²² $[\text{RhCl}(\text{ent-1})]_2$, and $[\text{RhCl}(\mathbf{2})]$ ²² revealed many similarities (Table 1). However, the following differences were detected. In the cationic monomer $[\text{RhOH}_2(\mathbf{2})]\text{SbF}_6$, the distance between the Rh atom and $\text{C8}=\text{C9}$, i.e., the enamide $\text{C}=\text{C}$ double bond, is significantly shorter than the distance between the Rh atom and $\text{C11}=\text{C12}$, i.e., the cyclopentene $\text{C}=\text{C}$ double bond. Only a very small difference was visible in the neutral monomer $[\text{RhCl}(\mathbf{2})]$,²² while the corresponding dimeric complexes possessed similar distances. In addition, a shorter Rh–Cl distance was observed for the monomeric complex: $[\text{RhCl}(\mathbf{1})]_2$, $[\text{RhCl}(\text{ent-1})]_2 > [(\text{Rh}(\mathbf{1}))_2\text{Cl}]\text{SbF}_6 > [\text{RhCl}(\mathbf{2})]$.

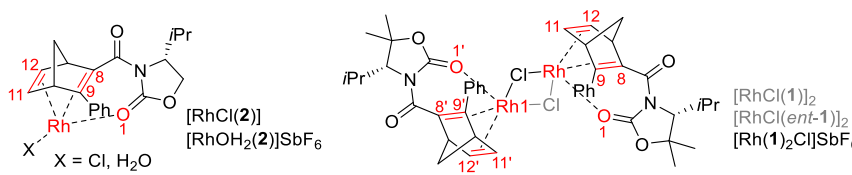
Electrochemical Investigations of the Rh Complexes.

In order to obtain information on the redox properties and particularly the redox equilibrium $\text{Rh}^{1+} \rightarrow \text{Rh}^{3+}$, the electrochemical behavior of the Rh complexes was studied by cyclic voltammetry. The cyclic voltammograms (CVs) (Figures S27–S30) showed only irreversible processes. However, the susceptibility toward oxidative deactivation could be inferred from the onset potential of the oxidation process (Table 2). The CV of the dimeric Rh–Cl complex $[\text{RhCl}(\mathbf{1})]_2$ showed $E_{\text{pa}} = 0.35$ V vs Fc/Fc^+ (the internal reference for all potentials reported herein), the monomeric Rh–Cl complex $[\text{RhCl}(\mathbf{2})]$ showed a shift $E_{\text{pa}} = 0.53$ V, and the CV of the monomeric Rh–OH₂ complex $[\text{RhOH}_2(\mathbf{2})]\text{SbF}_6$ had $E_{\text{pa}} = 1.59$ V, indicating that monomeric complexes in which the Cl ligands have been exchanged for water are more resistant to oxidation (entries 1–3). The CV of the monochloro dimer $[(\text{Rh}(\mathbf{1}))_2\text{Cl}]\text{SbF}_6$ showed $E_{\text{pa}} = 1.19$ V, which is in between those of the monomer and the dimer (entry 4).

From the higher redox stability of monomeric Rh complexes as compared to that of the dimeric counterparts, the following implications on their catalytic performance might be expected. Due to the fact that the Rh-catalyzed 1,2-additions to imines and 1,4-additions to enones are redox-neutral, i.e., the Rh^{1+} oxidation state is maintained throughout the catalytic cycle,^{24,21d} a higher redox stability of the monomeric complexes should correlate with a decreased tendency toward catalyst deactivation, resulting in higher yields.

XAS Investigations of the Rh Complexes. X-ray absorption spectroscopy (XAS) is particularly important to understand the behavior and potential structural changes of the dimeric and monomeric complexes in solution, which is directly connected to reactivity and selectivity, and XAS measurements have previously been very useful to give insight into the structures of Rh-olefin complexes.²⁵ Changes of XANES and EXAFS spectra from solid to solution should provide evidence for possible dimer/monomer equilibria or Cl^- dissociation. Thus, we measured XAS spectra at the Rh K-edge of the monomer $[\text{RhCl}(\mathbf{2})]$ and dimer $[\text{RhCl}(\mathbf{1})]_2$ both in the solid state and in 1,4-dioxane ($\text{C}_4\text{H}_8\text{O}_2$) solution (Figure 2a–d).

The XANES spectra of the monomeric complex $[\text{RhCl}(\mathbf{2})]$ in the solid state and in solution are nearly identical, having an edge energy that is 4.6(2.3) eV lower than that of Rh foil (Figure 2b). The edge energy in the XANES spectrum gives information about the oxidation state of the complex, where complexes in a

Table 1. Comparison of Selected Bond Distances (Å) and Angles (°) for Rh Complexes^a


	monomeric complexes			dimeric complexes		
	[RhOH ₂ (2)]SbF ₆ conformer A	[RhOH ₂ (2)]SbF ₆ conformer B	[RhCl(2)] ^b	[(Rh(1)) ₂ Cl]SbF ₆	[RhCl(ent-1)] ₂	[RhCl(1)] ₂ ^b
C8=C9	1.420(14)	1.445(14)	1.423(5)	1.482(8)	1.435(5)	1.429(3)
C11=C12	1.401(16)	1.386(15)	1.392(5)	1.405(8)	1.400(5)	1.397(3)
C8'=C9'				1.433(9)	sym. rel. ^c	sym. rel. ^c
C11'=C12'				1.393(9)	sym. rel. ^c	sym. rel. ^c
Rh → C8=C9	2.047(10)	2.049(10)	2.093(4)	2.115(7)	2.097(3)	2.0965(2)
Rh → C11=C12	2.107(10)	2.115(10)	2.070(3)	2.115(7)	2.102(3)	2.1065(2)
Rh → C8'=C9'				2.063(7)	sym. rel. ^c	sym. rel. ^c
Rh → C11'=C12'				2.054(6)	sym. rel. ^c	sym. rel. ^c
Rh–Cl			2.3292(9)	2.377(2)	2.4038(9)	2.4038(6)
Rh1–Cl				2.387(2)	2.4082(8)	2.4090(6)
Rh–Rh				3.5173(7)	2.9726(5)	3.0001(3)
Rh → O1	2.071(7)	2.101(7)	2.118(2)	2.081(4)	2.946(3)	2.939(2)
Rh1 → O1'				2.090(4)		
Rh → OH ₂	2.093(8)	2.086(8)				
C=O1	1.213(12)	1.235(13)	1.227(4)	1.216(8)	1.210(4)	1.199(3)
tilt angle ^d	−0.7(8)	−0.9(8)	−0.3(3)	−1.1(5) [−0.5(5)]	0.7(3)	−0.5(3)
bite angle ^e	81.4(4)	81.2(4)	81.9(2)	81.9(3) [81.8(3)]	81.2(1)	81.3(1)

^aAtom numbering only for comparison. ^bValues from ref 22. ^cSymmetry related (sym. rel.), dimeric system generated by the symmetry operator. ^dC8–C9–C11–C12 [C8'–C9'–C11'–C12'] defines the tilt angle. ^eC8–Rh–C11 [C8'–Rh1–C11'] defines the bite angle.

Table 2. Redox Potentials of Cationic and Neutral Rh Complexes

entry	complex	E_{pa} (oxidation)	E_{pc} (reduction)
1	[RhCl(2)]	0.53 V	−2.12 V
2	[RhOH ₂ (2)]SbF ₆	1.59 V	−1.93 V
3	[RhCl(1)] ₂	0.35 V	−1.93 V
4	[(Rh(1)) ₂ Cl]SbF ₆	1.19 V	−1.71 V

higher oxidation state typically have a higher edge energy. However, contrary to what is expected, monomer [RhCl(2)] has a lower energy than Rh(0). Using *ab initio* calculated spectra and local density of states (IDOS, where *l* = s, p, d, etc.) functions, contributions from 1s → 4d, 1s → 5p transitions, and ligand p-orbitals that mainly affect the edge shape were identified (for details, see the Supporting Information). The XANES spectra of the monomer suggest that the solution and solid-state structures are identical. In contrast, the XANES edge energy of the dimeric complex [RhCl(1)]₂ (Figure 2d) in the solid state is 5.0(2.3) eV lower than that of Rh foil, while in solution, it is 8.6(2.3) eV lower than that of Rh foil. Therefore, a change of the structure of the dimeric complex [RhCl(1)]₂ upon solvation is assumed.

More information about the structures is available from EXAFS spectra, which allow the identity of and distance to the nearest neighbor atoms to be determined. Figure 2a,c shows the experimental Fourier-transformed EXAFS spectra (R-space) in both the solid state and solution. First shell structural parameters obtained from the EXAFS spectra are given in Table 3. The first coordination shell (1.0–2.5 Å) of the monomer is composed of four types of scattering paths with four C, one O, and one Cl neighboring atoms but is dominated by the Rh–C scatter with a bond length of 2.051(7) Å for the solid sample and 2.055(6) Å for the solution (Figure 2a and Table 3). The distances are all in

good agreement with the crystallographic values for [RhCl(2)]. The fitted parameters of the solid and solution spectra show no significant differences.

The EXAFS spectra for the dimer [RhCl(1)]₂ in the solid state and in solution are presented in Figure 2c. The first shell signal of the solid-state sample is composed of four types of well-defined scattering paths, dominated by two Rh–C paths and one Rh–Cl path containing four and two backscattering atoms, respectively. The most important shells for the following section are those of Rh–Cl with two atoms at 2.44 Å and the Rh–Rh shell at 2.94 Å, both in very good agreement with the crystal structure (Table 1: Rh–Cl = 2.4038(6) Å and 2.4090(6) Å, Rh–Rh = 3.0001(3) Å; detailed results of dimeric samples in Tables S9 and S10). In the solution spectrum of the dimer [RhCl(1)]₂, the Rh–Rh shell is still present, clearly indicating a dimeric species in solution. However, the contribution of the Rh–Cl pair at a distance of 2.483(118) Å is negligible, as it exhibits an unphysically large Debye–Waller factor. The very large mean displacement of 0.0453(143) Å² for the Rh–Cl scatter (Table S10) suggests that at least one or even both Cl ligands are removed from the inner sphere of the Rh coordination, as supported by the very large uncertainty in the Cl coordination number of ±0.8. In addition, a new Rh–O scattering path is visible in the solution spectrum at 2.631(7) Å, which is not found in the solid complex (Table 3).

Based on the combined XANES and EXAFS data, we conclude that, while the monomeric species [RhCl(2)] has similar structures in the solid state and in solution, one or both bridging Cl[−] ligands are replaced by an O-containing ligand dioxane upon solvation of the dimeric species [RhCl(2)]₂, resulting in a cationic Rh(I) species. Such a change agrees with the EXAFS data, in which a Rh–Cl scattering path is replaced by a new Rh–O bond. This also explains the pronounced shift in

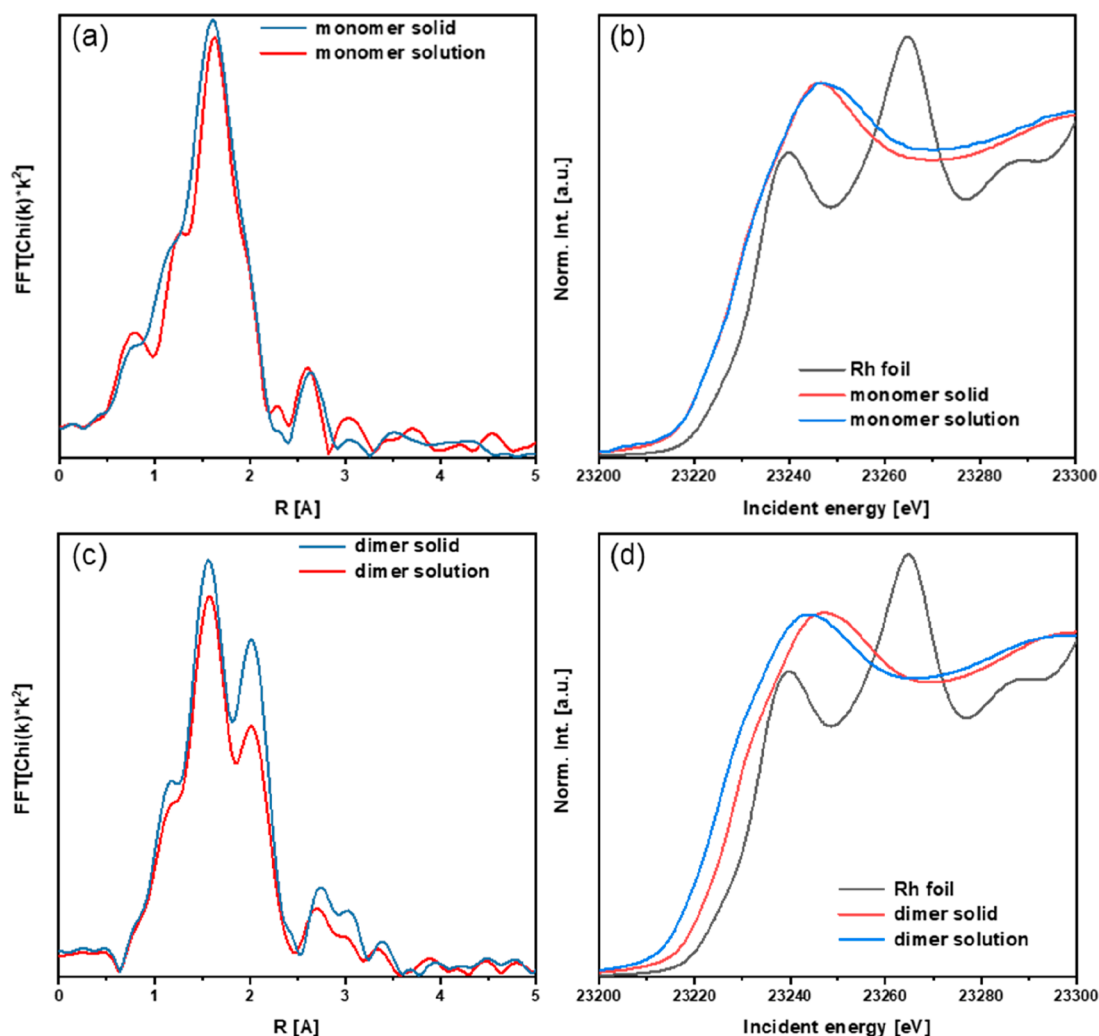


Figure 2. XAS spectra in both solution and solid state of the monomer $[\text{RhCl}(\text{2})]$ (a, EXAFS R-space spectra) (b, XANES) and dimer $[\text{RhCl}(\text{1})]_2$ (c, EXAFS R-space spectra) (d, XANES). XANES spectrum of a Rh(0) foil is shown as reference. The edge positions, EXAFS data in k -space, as well as the best fits are shown in Figures S4 and S5.

Table 3. First Shell Coordination Numbers (N) and Distances of $[\text{RhCl}(\text{2})]^\text{a}$ and $[\text{RhCl}(\text{1})]_2^\text{a}$

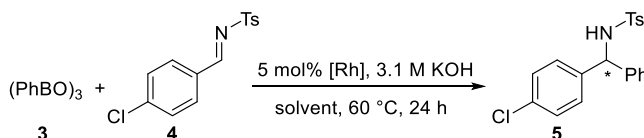
path	solid		solution		solid – solution
	N	$R + \Delta R$ (Å)	N	$R + \Delta R$ (Å)	
monomer					
Rh–O	2.2(5)	1.893(15)	1.3(2)	1.866(14)	0.027(29)
Rh–C	3.5(2)	2.051(7)	2.9(2)	2.055(6)	–0.004(13)
Rh–Cl	0.7(1)	2.251(6)	0.7(1)	2.248(12)	0.003(18)
Rh–C	3.4(4)	2.530(9)	2.8(4)	2.491(10)	0.039(19)
dimer					
Rh–C	1.0(1)	1.804(4)	1.0(1)	1.799(7)	0.005(11)
Rh–C	2.4(1)	2.094(3)	2.4(1)	2.079(4)	0.015(7)
Rh–C	2.4(1)	2.228(5)	2.3(1)	2.191(6)	0.037(11)
Rh–C	1.9(1)	2.409(7)	2.0(1)	2.311(8)	0.098(15)
Rh–Cl	2.1(1)	2.439(3)	2.0(8)	2.438(118)	–0.044(121)
Rh–O	-	-	2.0(1)	2.631(7)	-
Rh–Rh	0.8(1)	2.924(10)	0.7(1)	2.925(12)	0.017(22)

^aObtained by EXAFS fitting of samples of monomeric $[\text{RhCl}(\text{2})]$ and dimeric $[\text{RhCl}(\text{1})]_2$ in powder and in solution and calculated differences. For fitted E_0 and SO_2 parameters as well as the statistical evaluation of the fits, see the Supporting Information and Table S11.

XANES spectrum of the dissolved dimer $[\text{RhCl}(\text{1})]_2$, since a cationic species would result in bond contraction of the remaining ligands and thus increased mixing of the ligand p -orbitals with the Rh 4d-orbitals. Additionally, one could rationalize this shift as being due to exchange of a negatively charged Cl^- by dioxane, a higher-field ligand, leading to a more electron-rich Rh center, despite the positive charge.

DFT calculations at the B3LYP/def2-SVP-D3(BJ) level support this assumption. The replacement of chlorine by solvent molecules can directly be modeled. If one chloride is replaced by a water molecule to give $[(\text{Rh}(\text{1}))_2\text{Cl}\cdot\text{OH}_2]^+$, the complex opens somewhat, and the Rh–Rh distance increases from 3.297 Å in $[(\text{Rh}(\text{1}))_2\text{Cl}]^+$ to 4.128 Å in $[(\text{Rh}(\text{1}))_2\text{Cl}\cdot\text{OH}_2]^+$. The water attaches preferentially to one Rh ($\text{O}–\text{Rh} = 2.187$ Å) with a larger distance to the other Rh (3.704 Å). A similar situation was found with dioxane instead of water. Replacement of both chloride ions by water results effectively in the dissociation of the dimer in two monomers $[\text{RhOH}_2(\text{1})]^+$ with a Rh–Rh distance of 4.432 Å. Thus, one chloride ion is more likely to be exchanged for a solvent molecule than both in solution.

Catalytic 1,2-Additions. With the information on the structural features (from X-ray), stability toward oxidative

Table 4. Catalytic 1,2-Additions^a

entry	configuration		solvent	yield (%)		
	ligand	catalyst		NMR ^b	isolated	e.r. (R):(S)
1 ^c	(1R,4S,4'R)	<i>in situ</i> [RhCl(1)] ₂ ^d	dioxane	58	58	99:1
2	(1R,4S,4'R)	[RhCl(1)] ₂	dioxane	61	54	99:1
3	(1S,4R,4'S)	<i>in situ</i> [RhCl(<i>ent</i> -1)] ₂ ^d	dioxane	60	58	2:98
4	(1S,4R,4'S)	[RhCl(<i>ent</i> -1)] ₂	dioxane	77	70	2:98
5 ^c	(1R,4S,4'R)	<i>in situ</i> [RhCl(2)] ^d	dioxane	76	61	95:5
6	(1R,4S,4'R)	[RhCl(2)]	dioxane	76	58	96:4
7	(1R,4S,4'R)	[(Rh(1)) ₂ Cl]SbF ₆	dioxane	47	39	95:5
8	(1R,4S,4'R)	[RhOH ₂ (2)]SbF ₆	dioxane	66	61	94:6
9 ^c	(1R,4S,4'R)	<i>in situ</i> [RhCl(1)] ₂ ^d	ME ^e	77	65	98:2
10	(1R,4S,4'R)	[RhCl(1)] ₂	ME ^e	73	59	93:7
11	(1S,4R,4'S)	<i>in situ</i> [RhCl(<i>ent</i> -1)] ₂ ^d	ME ^e	72	71	27:73
12	(1S,4R,4'S)	[RhCl(<i>ent</i> -1)] ₂	ME ^e	96	90	9:91
13 ^c	(1R,4S,4'R)	<i>in situ</i> [RhCl(2)] ^d	ME ^e	93	84	61:39
14	(1R,4S,4'R)	[RhCl(2)]	ME ^e	91	86	25:75
15	(1R,4S,4'R)	[(Rh(1)) ₂ Cl]SbF ₆	ME ^e	65	52	92:8
16	(1R,4S,4'R)	[RhOH ₂ (2)]SbF ₆	ME ^e	96	78	58:42

^aThe active catalyst was generated by addition of a 3.1 M KOH solution to a solution of appropriate isolated Rh complex. After the mixture was heated to 60 °C, 3 and 4 were added (see Supporting Information). ^bMesitylene was used as the internal standard. ^cResults from ref 22. ^dThe catalyst was generated *in situ* by stirring a solution of ligand and precursor [RhCl(C₂H₄)₂]₂ for 15 min followed by addition of a 3.1 M KOH solution and stirring for a further 5 min (see Experimental Section). ^eMicroemulsion: 0.60 g of C₈G₁, 0.80 mL of toluene, 0.70 mL of H₂O.

decomposition (from CV), coordination sphere (from EXAFS), and oxidation state (from XANES) of the Rh complexes in hand, we compared their catalytic activity and enantioselectivity by using the 1,2-addition of triphenylboroxine 3 to 4-chlorobenzylidene-*N*-tosylimine 4 as a benchmark reaction. The comparative catalytic studies should answer the following questions: (a) does the catalytic performance differ between *in situ* formed and isolated complexes; is the catalytic activity and selectivity dependent on (b) the nuclearity or (c) the charge of the catalyst; (d) is there any beneficial influence of nanostructured solvents (i.e., microemulsions) as compared to conventional solvents such as dioxane?

First, a series of experiments were performed in dioxane (Table 4). Thus, triphenylboroxine 3 was treated with 4-chlorobenzylidene-*N*-tosylimine 4 in the presence of 0.2 equiv of KOH with a catalyst loading of 5 mol % [Rh] for 24 h at 60 °C to give product *N*-tosylamine 5 after column chromatography on silica. A comparison of the results in Table 4 reveals that the method of catalyst preparation had almost no impact on yields and enantiomeric ratios (entries 1–6). For the following experiments, isolated complexes were employed.

Yields differed only little between the different Rh complexes in dioxane giving *N*-tosylamine 5 in 54–70% (entries 2, 4, 6, 8) except for cationic dimeric complex [(Rh(1))₂Cl]SbF₆, which provided 5 in only 39% (e.r. 95:5, entry 7). The enantioselectivity was affected to some extent by the type of catalyst used. The enantiomeric ratio was higher for neutral dimeric complexes [RhCl(1)]₂ and [RhCl(*ent*-1)]₂ (e.r. = 99:1 and 2:98, entries 2, 4) than for the neutral monomeric complex [RhCl(2)] (e.r. 96:4, entry 6) or both cationic complexes [RhOH₂(2)]SbF₆ and [(Rh(1))₂Cl]SbF₆ (e.r. = 95:5 and 94:6, entries 7, 8).

In order to study whether the influence of the nuclearity and the charge of the catalyst on the catalytic activity and selectivity depends on the chosen reaction medium, catalysis was also run in a bicontinuously nanostructured microemulsion made of 28 wt % of C₈G₁ surfactant and equal amounts of toluene and water (for details, see the Supporting Information).²² The microemulsion promoted the catalytic efficiency, resulting in better yields as compared to dioxane. One might speculate that this effect relates to an improved activation of the Rh complex when residing in the amphiphilic film of the microemulsions.²² While the trend found for the yield, the use of microemulsions as reaction medium rather led to decreasing enantiomeric ratios (entries 9–16). For example, the neutral monomeric complex [RhCl(2)] gave 5 in 86% (e.r. 25:75) (entry 14) as compared to dioxane (58%, 96:4) (entry 6). In the case of the cationic monomeric complex [RhOH₂(2)]SbF₆, the microemulsion led to a nearly complete loss of stereocontrol, and 5 was isolated in 78% albeit with an e.r. = 58:42 (entry 16) as compared to dioxane (61%, e.r. = 94:6, entry 8).

Thus, the influence of nuclearity and charge of the Rh complexes were found to be moderate in dioxane, mostly affecting the enantiomeric ratios. In contrast, in the liquid confinement of microemulsions, the catalytic 1,2-addition is accelerated as compared to dioxane in agreement with previous kinetic experiments,²² but the stereocontrol is strongly affected by the nuclearity and even more by the charge, leading to almost racemic product 5 when cationic monomeric complex [RhOH₂(2)]SbF₆ was used in microemulsions, while the use of dioxane resulted in decent stereocontrol (entries 8, 16).

Investigation of Nonlinear Effects of Dimeric Rh Complexes in 1,2-Addition. As nonlinear effects have been reported for some diene ligands,¹⁷ we were curious whether mixtures of neutral dimeric complexes [RhCl(1)]₂ and

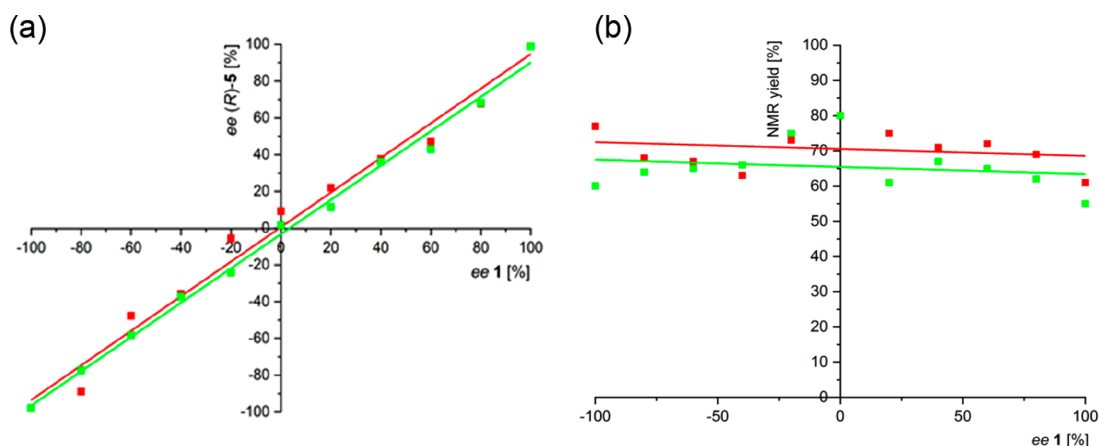


Figure 3. Dependency of the enantiomeric excess of *N*-tosylamine (*R*)-**5** (a) and yield (b) on the enantiomeric excess of ligand (1*R*,4*S*,4'*R*)-**1** (green) and dimeric Rh complex $[\text{RhCl}(\mathbf{1})]_2$ (red) in the catalytic 1,2-addition of triphenylboroxine **3** to 4-chlorobenzylidene-*N*-tosylimine **4**. For details of the reaction conditions, see Table 4.

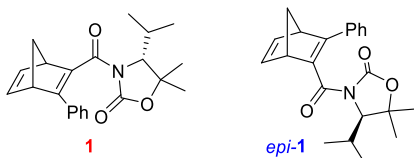
$[\text{RhCl}(\text{ent-1})]_2$ might show nonlinear effects in the asymmetric 1,2-addition, resulting in higher (or lower) ee values as would have been expected from the enantiomeric purity (%ee value) of the used ligands **1** or *ent-1*. Thus, mixtures of enantiomeric ligands **1** and *ent-1* in varying molar ratios were employed in the Rh-catalyzed 1,2-addition of triphenylboroxine **3** to 4-chlorobenzylidene-*N*-tosylimine **4** in dioxane in the presence of KOH under the *in situ* conditions. When the %ee of ligand **1** was plotted vs the %ee of product **5**, a linear correlation was found (Figure 3a, green line). The same was true when mixtures of isolated complexes $[\text{RhCl}(\mathbf{1})]_2$ and $[\text{RhCl}(\text{ent-1})]_2$ were employed (Figure 3a, red line).

In general, yields only slightly decreased for higher %ee values (Figure 3b). However, isolated complexes (Figure 3b, red line) performed better than the *in situ* generated species (Figure 3b, green line).

Since preliminary results²² showed that norbornadiene based ligands with low diastereomeric excesses led to high enantioselectivities in the Rh-catalyzed 1,2-addition of triphenylboroxine **3** to *N*-tosylimine **4**, there was a need to investigate possible nonlinear-like effects (NLLE), which have been previously described for catalytic 1,2-additions of diethylzinc to aldehydes in the presence of chiral *N,O*-[2.2]-paracyclophane ligands.²⁶ Therefore, the diastereomeric (1*R*,4*S*,4'*R*)-configured ligand **1** and (1*S*,4*R*,4'*R*)-configured epimeric *epi-1* were mixed in different molar ratios, the rhodium precursor $[\text{RhCl}(\text{C}_2\text{H}_4)_2]_2$ was added, and the formed catalysts were submitted to the catalytic 1,2-addition of **3** to **4** in dioxane in the presence of KOH. Subsequently, the dependency of the enantiomeric excess of (*R*)-**5** on the diastereomeric excess of (1*R*,4*S*,4'*R*)-configured **1** was investigated (Scheme 2 and Figure 4).

Despite several attempts, only (1*R*,4*S*,4'*R*)-configured ligand **1** provided a crystalline Rh complex, whereas epimeric ligand *epi-1* gave no crystalline Rh complex, and thus, NLLE

Scheme 2



experiments were only carried out with the *in situ* formed Rh complexes of ligands **1** and *epi-1*.

When diastereomerically pure ligand **1** was applied, (*R*)-**5** was obtained in good yields with a high enantioselectivity (61%, 97%ee (*R*), blue circles), whereas diastereomerically pure ligand *epi-1* selectively formed (*S*)-**5** with surprisingly low yields (26%, 90%ee (*S*), red circles) (Figure 4a,b). When the diastereomeric excess (de) of **1** was lowered by adding increasing amounts of *epi-1*, the enantiomeric excess of (*R*)-**5** slowly decreased in an almost linear fashion until approximately 50%de was reached at -20%de.

A further decrease of the diastereomeric excess down to -96%de had no influence on the enantiomeric excess of (*R*)-**5**; however, yields significantly decreased further. At diastereomeric excesses below -96%de, the enantiomeric ratio suddenly dropped to the initial value, obtained with diastereomerically pure *epi-1*. The pronounced deviation of the %de of **1** vs %ee of (*R*)-**5** curve and the %de **1** vs NMR yield of (*R*)-**5** from linearity suggest a strong nonlinear-like effect. The NLLE might be caused by the interaction between a highly selective and highly reactive diastereomer $[\text{RhCl}(\mathbf{1})]_2$ with a less selective and weakly reactive diastereomer $[\text{RhCl}(\text{epi-1})]_2$, presumably through dimeric Rh complexes with mixed ligands. However, in NMR experiments with mixtures of two different Rh complexes, no ligand scrambling was observed, and thus, mixed dimers could be ruled out (Figure S1).

Catalytic 1,4-Additions. The catalytic 1,4-addition to enones **6** is a second benchmark reaction to assess the potential of novel diene ligands in asymmetric catalysis. In a similar fashion as was described above for the 1,2-addition, the following issues were probed: (a) performance of *in situ* formed vs isolated catalysts, catalytic performance with respect to the (b) nuclearity and (c) charge of the catalyst. Therefore, in a second series of experiments, the catalytic 1,4-addition of phenylboronic acid **7** to cyclopentenone **6a** and cyclohexenone **6b** was studied (Table 5).

It should be noted that the influence of nanoconfined reaction media, i.e., microemulsion vs conventional solvents, was also examined. As decent yields and enantioselectivities were only found in dioxane (Table S4), other solvents were not further considered. For example, reaction of cyclopentenone **6a** with **7** catalyzed by the monomeric complex $[\text{RhCl}(\mathbf{2})]$, which was *in situ* formed from $[\text{RhCl}(\text{C}_2\text{H}_4)_2]_2$ (1.7 mol %) and the diene

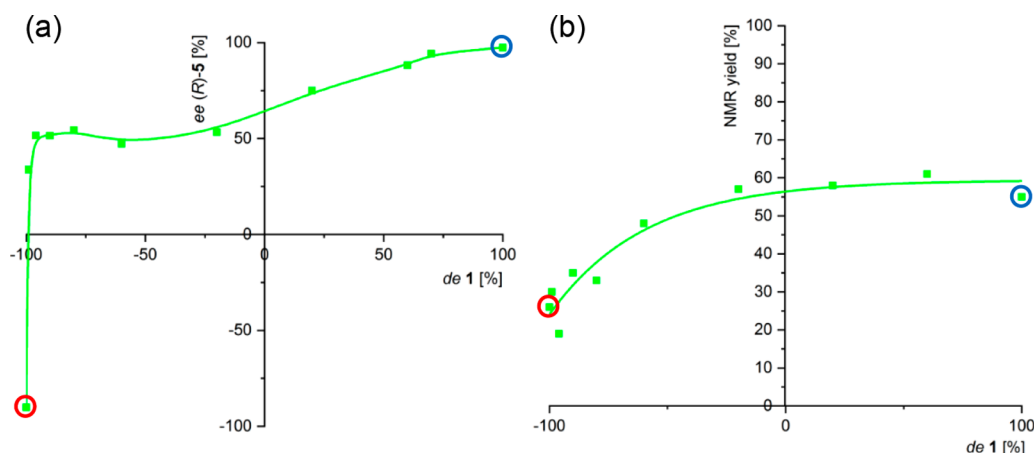


Figure 4. Dependency of the enantiomeric excess of *N*-tosylamine (*R*)-5 (a) and the yield (b) on the diastereomeric excess of ligand (1*R*,4*S*,4'*R*)-1 in the catalytic 1,2-addition of triphenylboroxine 3 to 4-chlorobenzylidene-*N*-tosylimine 4 using *in situ* formed Rh complexes. For details of the reaction conditions, see Table 4.

Table 5. Catalytic 1,4-Additions

entry	catalyst ^a	prod.	yield (%)		e.r. ^c (<i>R</i>):(<i>S</i>)
			NMR ^b	isolated	
1	<i>in situ</i> [RhCl(1)] ₂	8a	27	17	16:84
2	[RhCl(1)] ₂	8a	52	42	8:92
3	<i>in situ</i> [RhCl(<i>ent</i> -1)] ₂	8a	30	29	81:19
4	[RhCl(<i>ent</i> -1)] ₂	8a	43	27	75:25
5	[(Rh(1)) ₂ Cl]SbF ₆	8a	62	44	13:87
6	<i>in situ</i> [RhCl(2)]	8a	62	52	3:97
7	[RhCl(2)]	8a	70	66	5:95
8	[RhOH ₂ (2)]SbF ₆	8a	62	62	8:92
9	<i>in situ</i> [RhCl(1)] ₂	8b	33	27	61:39
10	[RhCl(1)] ₂	8b	38	27	65:35
11	<i>in situ</i> [RhCl(<i>ent</i> -1)] ₂	8b	44	44	50:50
12	[RhCl(<i>ent</i> -1)] ₂	8b	32	29	33:67
13	[(Rh(1)) ₂ Cl]SbF ₆	8b	19	21	50:50
14	<i>in situ</i> [RhCl(2)]	8b	52	46	31:69
15	[RhCl(2)]	8b	42	34	37:63
16	[RhOH ₂ (2)]SbF ₆	8b	48	46	32:68

^aFor catalyst preparation, see the Experimental Section and Supporting Information; ligand 1 and 2 are (1*R*,4*S*,4'*R*)-configured, ligand *ent*-1 is (1*S*,4*R*,4'*S*)-configured. ^bFor NMR yields, mesitylene was used as the internal standard. ^cThe main enantiomer was identified by specific rotation value measurement of the most enantioenriched product mixture.

ligand (1*R*,4*S*,4'*R*)-2 (3.4 mol %) in the presence of 3.1 M KOH at 50 °C, gave 2-phenylcyclopentanone 8a in 52% yield with an enantioselectivity of 3:97 in favor of the (*S*)-product (entry 6).

Slightly improved yields were observed for the isolated complex with a similar enantiomeric ratio (entry 7). In the case of neutral dimeric complex [RhCl(1)]₂, *in situ* conditions led to a considerable decrease of both yield and enantioselectivity (17%, e.r. = 16:84) (entry 1) as compared to the isolated dimer (42%, e.r. = 8:92) (entry 2). When the enantiomeric dimer [RhCl(*ent*-1)]₂ was used, the (*R*)-product (*R*)-8a was favored,

irrespective of the complex preparation method (entries 3 and 4).

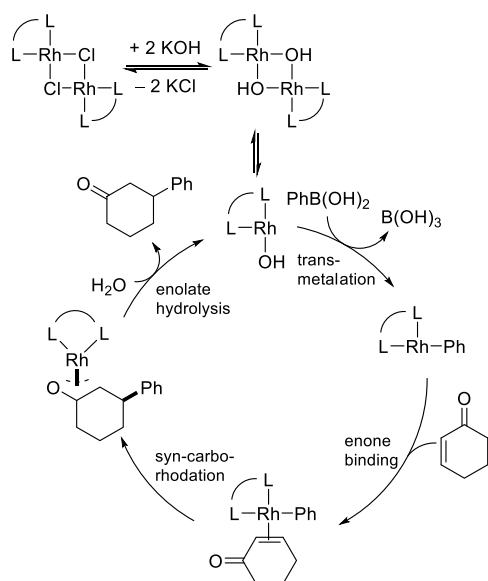
With regard to reactivity and selectivity, ligand 2, resulting in monomeric complexes [RhCl(2)] and [RhOH₂(2)]SbF₆, performed better than ligand 1, giving dimeric complexes [RhCl(1)]₂ and [(Rh(1))₂Cl]SbF₆ (entries 7 and 8 vs entries 2 and 5). In addition, neutral complexes performed slightly better than cationic complexes regarding yield and %ee. For example, neutral monomer [RhCl(2)] provided 8a in 66% yield and good enantioselectivity (e.r. = 5:95, entry 7) as compared to the corresponding isolated cationic monomer [RhOH₂(2)]SbF₆ (62%, e.r. = 8:92) (entry 8), while for the cationic dimer [(Rh(1))₂Cl]SbF₆, the yield and enantiomeric ratio decreased (44%, e.r. = 13:87) (entry 5).

However, the outcome was completely different, when cyclohexenone 6b was employed as a substrate. To our surprise, both yields and enantioselectivities decreased considerably as compared to the corresponding reactions with cyclopentenone 6a, irrespective of the use of *in situ* or isolated neutral complexes (entries 9–12, 14, and 15). In the case of isolated neutral dimer [RhCl(1)]₂, the enantioselectivity was reversed, now favoring the (*R*)-product (*R*)-8b (27%, e.r. = 65:35) (entry 10). Similar behavior was observed for the enantiomeric dimer complex [RhCl(*ent*-1)]₂ now yielding a racemic mixture (44%, e.r. = 50:50) via an *in situ* method and the (*S*)-product (*S*)-8b (29%, e.r. = 33:67) via an isolated complex (entries 11 and 12). Poor yields and low enantiomeric ratios were also observed for the cationic monomer [RhOH₂(2)]SbF₆ (entry 16) and the cationic dimer [(Rh(1))₂Cl]SbF₆ (entry 13). In the latter case, racemic 8b was obtained.

The erosion of stereoselectivity upon changing the substrate cyclopentenone 6a to cyclohexenone 6b irrespective of the type of catalyst was rather unexpected. According to the commonly accepted catalytic cycle^{20e} the monomeric hydroxo-Rh complex Rh-OH undergoes transmetalation with phenylboronic acid to the monomeric phenyl-Rh complex Rh-Ph (Scheme 3).

Subsequent enone binding delivers the phenyl-enone Rh complex (η^2 -enone)Rh-Ph, followed by rate-limiting carborhodation and final enolate hydrolysis. We surmised that this lack of stereocontrol might be caused by a higher conformational mobility of cyclohexenone 6b and smaller energetic differences between the various binding modes of the phenyl-Rh complex during enone binding. In order to validate this hypothesis, the

Scheme 3



enone binding step was examined by DFT methods for both complexes $[\text{Rh}(\mathbf{1})\text{-Ph}]$ and $[\text{Rh}(\mathbf{2})\text{-Ph}]$ derived from dimeric catalyst $[\text{RhCl}(\mathbf{1})]_2$ and monomeric catalyst $[\text{RhCl}(\mathbf{2})]$, respectively.

Enone Binding and Carborhodation Studied by DFT Calculations. To elucidate the mechanism and the stereocontrol of 1,4-additions, we studied the enone binding to the complexes $[\text{Rh}(\mathbf{1})\text{-Ph}]$ and $[\text{Rh}(\mathbf{2})\text{-Ph}]$ by DFT. They both include a phenyl ligand, which results from phenylboronic acid **7** by transmetalation (see Scheme 3). Both complexes are neutral and have a closed-shell electronic structure.

Enone binding can happen in different binding modes. In order to identify the most probable mechanism, i.e., the one with the lowest barrier, we had to study all of them. We identified four distinct binding modes (Figure 5). Each of these can be approached by the enone in a Re or a Si orientation, resulting in (*R*)-**8** and (*S*)-**8** products, respectively. In the binding modes, which lead to the lowest-energy transition states ($\eta^2\text{-cis}$, $\eta^2\text{-trans}$), the enone substrate is associated in an η^2 manner to rhodium (Rh–C distances = 2.19–2.36 Å), while the coordination of Rh to the oxazolidinone oxygen (O1 in Figure 5) is weakened (Rh–O distances = 2.52–3.13 Å). In the ring and phenyl binding modes (Figure 5), the oxazolidinone oxygen is bound to a different side of Rh with distances of 2.15–2.17 Å.

With the possible binding modes identified, we studied the carborhodation mechanism. Four binding modes and two Re/Si

orientations result in eight different reaction paths for cyclopentenone **6a**. In the case of cyclohexenone **6b**, the six-membered ring has an additional degree of freedom of the C5 atom pointing up or down with respect to the ring plane. Thus, 16 paths have to be distinguished for cyclohexenone **6b**. We studied all of them.

Of these 8 paths for 1,4-addition to 2-cyclopentenone **6a** with $[\text{Rh}(\mathbf{1})\text{-Ph}]$ as the catalytic intermediate, four transition states (the η^2 -ones, those with the lowest energies) are shown in Figure 6. The $\eta^2\text{-trans}$ binding resulted in the lowest free-energy barrier for the (*R*)-product ($\Delta G = 80$ kJ/mol), and $\eta^2\text{-cis}$ binding resulted in the lowest free-energy barrier for the (*S*)-product ($\Delta G = 67$ kJ/mol), see Table 6 and Figure 6. The significant energy difference of $\Delta\Delta G = 12.6$ kJ/mol results in a large predicted e.r. of 1:99 (*R*):(*S*). This agrees reasonably with the results in Table 5 (16:84, entry 1 and 8:92, entry 2). It confirms the significant stereoselectivity of Rh(**1**) for **6a**.

Of the 16 paths for 1,4-addition to cyclohexenone **6b** with $[\text{Rh}(\mathbf{1})\text{-Ph}]$ as the catalytic intermediate, η^2 binding again led to the lowest free-energy barriers. In contrast to **6a**, the barrier heights for (*R*)- and (*S*)-products are more similar, however. This time, the lowest barrier for the (*R*)-product (*R*)-**8b** ($\Delta G = 66$ kJ/mol, $\eta^2\text{-cis-up}$) is slightly lower than the lowest barrier for the (*S*)-product (*S*)-**8b** ($\Delta G = 68$ kJ/mol, $\eta^2\text{-trans-up}$). These result in a $\Delta\Delta G$ of merely 1.3 kJ/mol, corresponding to a predicted e.r. of 61:39 (*R*):(*S*), which compares very well to Table 5 (entries 9 and 10, 61:39 and 65:35). Again, the calculations confirm the experimental finding of low stereoselectivity Rh(**1**) for **6b**.

For $[\text{Rh}(\mathbf{2})\text{-Ph}]$, we investigated the reactivity with 2-cyclopentenone **6a**. Consistently with the other cases, the η^2 binding mode resulted in the lowest barriers. Those were $\Delta G = 80$ kJ/mol for the (*R*)-product (*R*)-**8a** ($\eta^2\text{-trans}$) and $\Delta G = 72$ kJ/mol for the (*S*)-product (*S*)-**8a** ($\eta^2\text{-cis}$), resulting in an e.r. of 6:94, compared to 3:97 and 5:95 from entries 6 and 7 of Table 5. Thus, independently of the catalyst, the (*S*)-product is favored for cyclopentenone **6a**.

In order to rationalize the different stereoselectivity found for **6a** vs **6b**, the structures of the transition states are illustrated in Figure 6. Re and Si structures are superimposed. The alignment of the substrate, especially its enone O, differs much more between the Re and Si structures for **6a** (top row) than for **6b** (bottom row). The more flexible six-membered ring of **6b** leads to similar positions of the enone O in Re and Si structures, reducing the difference in barrier height and, thus, the stereoselectivity. The stiffer five-membered ring of **6a** leads to more distinctive structures. In the $\eta^2\text{-cis}$ structures (Figure 6, left) the positive partial charge, which accumulates at the enone-O during the reaction, seems to be stabilized by an interaction of

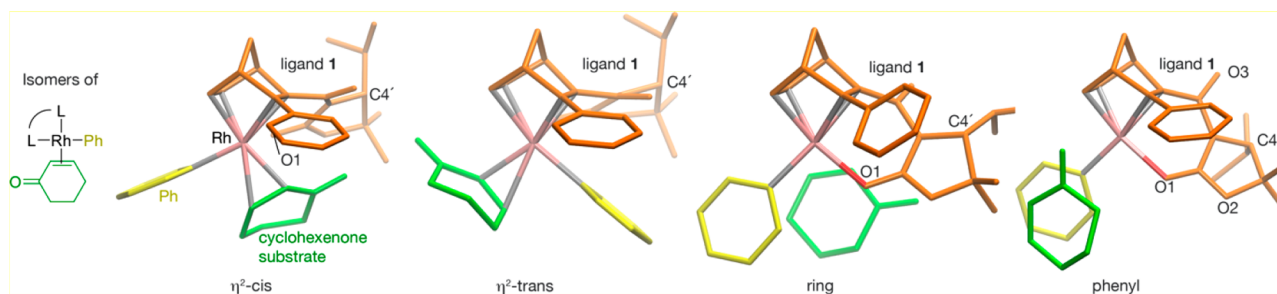


Figure 5. Four distinct enone binding modes of 2-cyclohexenone **6b** to $[\text{Rh}(\mathbf{1})\text{-Ph}]$, which results from $[\text{RhCl}(\mathbf{1})]_2 + \mathbf{7}$. Hydrogen atoms are omitted for clarity. The norbornadiene ligand is orange, the phenyl ligand is yellow, and the cyclohexenone substrate is green.

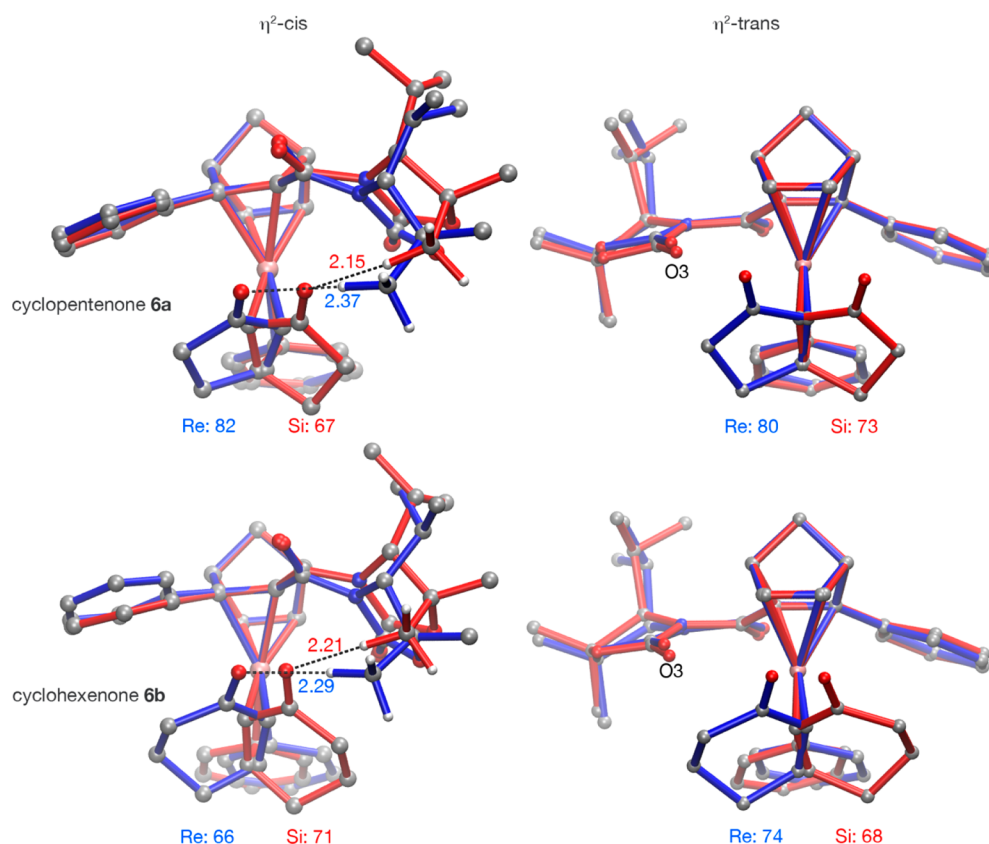


Figure 6. Comparison of the transition states for carborhodation of 2-cyclopentenone **6a** (top) and 2-cyclohexenone **6b** (bottom) with [Rh(1)-Ph]. The left structures show the η^2 -cis mechanism, and the right ones show the η^2 -trans mechanism. The transition states resulting in the (*R*)-products (*R*)-**8a,b** are blue, and those that result in the (*S*)-products (*S*)-**8a,b** are red. Most hydrogen atoms are omitted for clarity. Specific bond lengths are shown in Å, and the barrier heights for Re and Si transition states are shown in kJ/mol.

Table 6. Barriers for the 1,4-Additions via Catalytic Intermediates [Rh(1)-Ph] and [Rh(2)-Ph]

reactants	binding mode with lowest barrier		barrier (ΔG in kJ/mol)		e.r. (<i>R</i>):(<i>S</i>)
	Re	Si	Re	Si	
6b + [Rh(1)-Ph]	η^2 -cis-up	η^2 -trans-up	66	68	61:39
6a + [Rh(1)-Ph]	η^2 -trans	η^2 -cis	80	67	1:99
6a + [Rh(2)-Ph]	η^2 -trans	η^2 -cis	80	72	6:94

the methyl groups bound to C5' of the ligand (**1**). In all four structures, rather short distances, reminiscent of hydrogen bonds, are observed. For **6a**, they differ significantly between 2.37 Å for Re and 2.15 Å for Si, while they are with 2.29 and 2.21 Å more similar for **6b**. Ligand (**2**) misses these methyl groups. Their influence is corroborated by the lower enantioselectivity found with (**2**) than with (**1**). In η^2 -trans, there is a possibly unfavorable interaction between the enone O and the (also negatively charged) O3 atom of the oxazolidinone ring of the ligand (**1**), which is present for the Re structures, but not for the Si structures (Figure 6). Again, this interaction is much stronger for the stiff **6a** than the flexible **6b**. Overall, subtle nonbonding interactions lead to a stabilization of the negative charge, which accumulates on the enone-O of the substrate during the reaction. This stabilization differs more between the stereoisomers in the smaller and stiffer **6a** than in the more flexible **6b**, which explains the higher stereoselectivity.

CONCLUSION

We have synthesized two novel cationic dimeric and monomeric chiral Rh diene complexes [(Rh(**1**))₂Cl]SbF₆ and [RhOH₂(**2**)]SbF₆ from structurally closely related oxazolidinone-norbornadiene ligands **1** and **2**, which we compare to their neutral counterparts [RhCl(**1**)]₂ and [RhCl(**2**)].²²

The solid-state structure, as determined by X-ray diffraction, differed little between cationic and neutral Rh complexes. XANES revealed slight differences in the local geometry at the Rh center between the dimeric complex [RhCl(**1**)]₂ and the monomeric complex [RhCl(**2**)].

In solution, the electronic structure of Rh remains similar to the solid state, as found by XANES. According to the EXAFS data, the overall dimeric structure of [RhCl(**1**)]₂ is preserved in solution; however, one (or both) of the bridging chloro ligands are replaced by the solvent dioxane, which is in agreement with previous findings in Rh-catalyzed Pauson-Khand cyclizations.²⁷ This observation agrees well with the commonly accepted catalytic cycle for Rh-diene-catalyzed asymmetric nucleophilic additions,^{20g} where the chloro-bridged dimeric Rh complex is first converted to the hydroxo-bridged dimeric Rh complex and then breaks down to the catalytically active monomeric diene Rh–OH species.

The catalytic activity and enantioselectivity of the Rh complexes were investigated in the Rh-catalyzed asymmetric 1,2-addition of triphenylboroxine **3** to *N*-tosylimine **4** and the 1,4-addition of phenylboronic acid **7** to cyclopentenone **6a** or cyclohexenone **6b**. The following trends were observed for the 1,2-addition: Higher yields were obtained for ligand **2** than

ligand **1**, and higher enantioselectivity was obtained for ligand **1** for both, the cationic and the neutral complexes. The higher yields for ligand **2** correlate well with their increased electrochemical oxidation stability determined by their higher onset oxidation potential in cyclic voltammetry, which increased in the series $[\text{RhCl}(\mathbf{1})_2] < [\text{RhCl}(\mathbf{2})] < [(\text{Rh}(\mathbf{1}))_2\text{Cl}]\text{SbF}_6 < [\text{RhOH}_2(\mathbf{2})]\text{SbF}_6$. When comparing neutral vs charged complexes, the neutral monomer gave better yields and enantioselectivities, while the difference for the neutral and charged dimers was only marginal.

The liquid confinement in microemulsions produced higher yields than dioxane but lower enantioselectivities, which might be related to the different orientation of the Rh complexes in/near the amphiphilic film compared to unstructured dioxane.

A strong positive nonlinear-like effect (NLLE) regarding diastereomeric excess of **1** and *epi-1* was found in the diastereomeric mixture of $[\text{RhCl}(\mathbf{1})_2]$ and $[\text{RhCl}(\textit{epi-1})_2]$, while no such effect was found for varying enantiomeric purity between $[\text{RhCl}(\mathbf{1})_2]$ and $[\text{RhCl}(\textit{ent-1})_2]$.

In the 1,4-addition to cyclopentenone **6a**, complexes with ligand **2** (both neutral and cationic) gave higher yields and enantioselectivities than the corresponding complexes with ligand **1**. The poorer performance of ligand **1** can be rationalized by the additional *gem*-dimethyl group of **1** as compared to **2**, which seems to be far away from the Rh center according to the X-ray data (Figure 1) but is close (2.15 Å) to the substrate in the main transition state according to DFT calculations (Figure 6). The 1,4-addition turned out to be strongly substrate-dependent, giving very low enantioselectivity and, in several cases, racemic products when cyclohexenone **6b** was employed as substrate. DFT calculations explained this by showing that the negative partial charge accumulating at the substrate O is more efficiently stabilized in the (*R*)-transition states in the more rigid **6a** than in the more flexible **6b**.

This combined experimental and theoretical study demonstrated that for chiral oxazolidinone-substituted norbornadiene ligands **1**, *ent-1*, and **2** there is no “one size fits all” Rh catalyst. We found and explained remarkably different reactivities and selectivities depending on the specific reaction type, substrate, and solvent between both monomeric and dimeric complexes $[\text{RhCl}(\mathbf{2})]$ and $[\text{RhCl}(\mathbf{1})_2]$ and their cationic counterparts $[\text{RhOH}_2(\mathbf{2})]\text{SbF}_6$ and $[(\text{Rh}(\mathbf{1}))_2\text{Cl}]\text{SbF}_6$. The current results paved the way to further exploration of monomeric Rh complexes in asymmetric catalysis.

EXPERIMENTAL SECTION

General Methods. All reactions were run under a nitrogen atmosphere in flame-dried glassware using standard Schlenk techniques. NMR spectra were recorded on a 500 MHz Bruker Avance 500 or a 700 MHz Bruker Avance 700 NMR spectrometer, referenced to tetramethylsilane (δ 0.00 ppm) and calibrated on the residual solvent peaks. Mass spectra were recorded with a Bruker Daltonics micro-TOF-Q using electrospray ionization (ESI) with nitrogen as carrier gas. Dioxane was degassed by bubbling nitrogen through it. All other solvents and reagents were used as purchased. Diene ligands were synthesized according to the literature.²²

Synthesis of $[\text{RhCl}(\textit{ent-1})_2]$. Diene ligand *ent-1* (67.4 mg, 0.19 mmol) and $[\text{RhCl}(\text{C}_2\text{H}_4)_2]_2$ (37.3 mg, 95.9 μmol) were loaded in a Schlenk tube under a nitrogen atmosphere, dioxane (2 mL) was added, and the reaction mixture was stirred for 5 h at room temperature. The remaining solids were filtered off, and the solvent was removed under reduced pressure. After recrystallization from Et_2O , the diene complex was obtained as a red solid (69.0 mg, 73%). ^1H NMR (500 MHz, CDCl_3): δ 7.71–7.64 (m, 4H), 7.33–7.27 (m, 6H), 4.70–4.64 (m, 2H), 4.51–4.45 (m, 2H), 4.42–4.38 (m, 2H), 3.91 (d, $J = 3.6$ Hz, 2H),

3.88–3.82 (m, 2H), 2.32–2.21 (m, 2H), 1.68 (dt, $J = 1.4, 9.8$ Hz, 2H), 1.46 (dt, $J = 1.4, 9.8$ Hz, 2H), 1.37 (s, 6H), 1.14 (d, $J = 7.3$ Hz, 6H), 1.07 (d, $J = 7.3$ Hz, 6H), 0.62 (s, 6H) ppm. ^{13}C $\{^1\text{H}\}$ NMR (176 MHz, CDCl_3): δ 167.4, 158.4, 137.4, 129.0, 128.2, 128.1, 87.1, 69.6, 63.4, 60.7, 59.7, 58.5 (d, $J = 11.5$ Hz), 56.1, 53.8 (d, $J = 10.4$ Hz), 44.1, 29.5, 27.6, 21.7, 20.9, 17.7 ppm. LRMS (ESI) calcd m/z for $[\text{M} - \text{Cl}]^+$ 943.1, found m/z 943.1. HRMS (ESI) calcd (found) for $\text{C}_{44}\text{H}_{50}\text{ClN}_2\text{O}_6\text{Rh}_2$ ($[\text{M} - \text{Cl}]^+$): 943.1462 (943.1471). Anal. Calcd (%) for $\text{C}_{44}\text{H}_{50}\text{Cl}_2\text{N}_2\text{O}_6\text{Rh}_2$ (979.62 g/mol): C: 53.95; H: 5.15; N: 2.86. Found: C: 54.02; H: 5.42; N: 2.68.

Synthesis of $[(\text{Rh}(\mathbf{1}))_2\text{Cl}]\text{SbF}_6$. Under a nitrogen atmosphere, $[\text{RhCl}(\mathbf{1})_2]$ (50.0 mg, 51.0 μmol) was dissolved in CH_2Cl_2 (5 mL), and AgSbF_6 (17.6 mg, 51.0 μmol) was added. The reaction mixture was stirred for 30 min at room temperature and filtered through Celite, and the solvent was removed under reduced pressure. The crude product was washed with hexanes (5 mL), and the cationic diene complex was obtained as a yellow solid (60.1 mg, quant.) without further purification. ^1H NMR (700 MHz, CD_2Cl_2): δ 7.86–7.57 (m, 4H), 7.46–7.16 (m, 6H), 4.76–4.69 (m, 2H), 4.54–4.49 (m, 2H), 4.48–4.43 (m, 2H), 4.01 (d, $J = 3.1$ Hz, 2H), 3.93–3.87 (m, 2H), 2.35–2.23 (m, 2H), 1.71 (dt, $J = 1.3, 6.9$ Hz, 2H), 1.44 (dt, $J = 1.3, 6.9$ Hz, 2H), 1.38 (s, 6H), 1.17 (d, $J = 7.3$ Hz, 6H), 1.08 (d, $J = 7.3$ Hz, 6H), 0.64 (s, 6H) ppm. ^{13}C $\{^1\text{H}\}$ NMR (176 MHz, CD_2Cl_2): δ 166.8, 159.8, 136.8, 129.6, 129.1, 127.9, 89.0, 70.1, 63.2 (d, $J = 12.6$ Hz), 61.5 (d, $J = 10.2$ Hz), 61.2, 60.3 (d, $J = 5.7$ Hz), 57.2, 55.9 (d, $J = 9.5$ Hz), 42.2 (d, $J = 11.5$ Hz), 29.8, 27.7, 21.6, 21.0, 17.4 ppm. LRMS (ESI) calcd m/z for $[\text{M} - \text{SbF}_6]^+$ 943.2, found m/z 943.2. HRMS (ESI) calcd (found) for $\text{C}_{44}\text{H}_{50}\text{ClN}_2\text{O}_6\text{Rh}_2$ ($[\text{M} - \text{SbF}_6]^+$): 943.1462 (943.1466). Anal. Calcd (%) for $\text{C}_{44}\text{H}_{50}\text{ClN}_2\text{O}_6\text{Rh}_2\text{SbF}_6 \cdot 1\text{H}_2\text{O}$ (1179.92 g/mol): C: 44.12; H: 4.38; N: 2.34. Found: C: 44.30; H: 4.58; N: 2.34.

Synthesis of $[\text{RhOH}_2(\mathbf{2})]\text{SbF}_6$. Under a nitrogen atmosphere, $[\text{RhCl}(\mathbf{2})]$ (0.10 g, 0.22 mmol) was dissolved in CH_2Cl_2 (4 mL), and AgSbF_6 (74.4 mg, 0.22 mmol) was added. The reaction mixture was stirred for 30 min at room temperature and filtered through Celite, and the solvent was removed under reduced pressure. The crude product was washed with hexanes (5 mL), and the cationic diene complex was obtained as a yellow solid (0.15 g, quant.) without further purification. ^1H NMR (700 MHz, CD_2Cl_2): δ 7.79–7.65 (m, 2H), 7.49–7.33 (m, 3H), 4.70–4.64 (m, 1H), 4.61–4.56 (m, 1H), 4.54–4.49 (m, 1H), 4.38–4.34 (m, 1H), 4.23 (dd, $J = 2.1, 9.5$ Hz, 1H), 4.13–4.07 (m, 1H), 3.87–3.83 (m, 1H), 2.66–2.58 (m, 1H), 2.42 (s, 2H), 1.64 (dt, $J = 1.4, 9.8$ Hz, 1H), 1.48 (dt, $J = 1.4, 9.8$ Hz, 1H), 0.96 (d, $J = 7.3$ Hz, 3H), 0.92 (d, $J = 7.3$ Hz, 3H) ppm. ^{13}C $\{^1\text{H}\}$ NMR (176 MHz, CD_2Cl_2): δ 166.4, 161.3, 136.0, 129.9, 129.5, 127.6, 67.9, 66.9 (d, $J = 10.7$ Hz), 63.0, 61.1, 60.4 (d, $J = 10.7$ Hz), 59.8 (d, $J = 7.7$ Hz), 56.9 (d, $J = 7.7$ Hz), 55.5, 32.7, 29.4, 18.0, 14.7 ppm. LRMS (ESI) calcd m/z for $[\text{M} - \text{SbF}_6]^+$ 444.1, found m/z 444.1. HRMS (ESI) calcd (found) for $\text{C}_{20}\text{H}_{23}\text{NO}_4\text{Rh}$ ($[\text{M} - \text{SbF}_6]^+$): 444.0677 (444.0679). Anal. Calcd (%) for $\text{C}_{44}\text{H}_{50}\text{ClN}_2\text{O}_6\text{Rh}_2\text{SbF}_6$ (680.06 g/mol): C: 35.32; H: 3.41; N: 2.06. Found: C: 35.22; H: 3.53; N: 1.84.

General Procedure for Addition Reactions with *In Situ* Prepared Catalyst. Under a nitrogen atmosphere, the appropriate ligand (10.0 μmol) and $[\text{Rh}(\text{C}_2\text{H}_4)_2\text{Cl}]_2$ (5.00 μmol) were dissolved in degassed dioxane (2 mL), and the solution was stirred for 15 min at room temperature. A degassed 3.1 M KOH solution (51.0 μL , 0.15 mmol) was added, and the reaction mixture was stirred for another 5 min at room temperature. In the case of 1,2-addition, the solution was heated to 60 °C, triphenylboroxine **3** (74.8 mg, 0.24 mmol) and *N*-tosylimide **4** (58.8 mg, 0.20 mmol) were added, and the reaction mixture was stirred for a further 24 h at 60 °C. After dilution with EtOAc (2 mL), the solution was filtered through a short silica column, the solvent was removed under reduced pressure, and the crude product was purified by column chromatography on silica. In the case of 1,4-addition, the solution was heated to 50 °C, phenylboronic acid **7** (74.0 mg, 0.60 mmol) and the respective enone **6a,b** (0.30 mmol) was added, and the reaction mixture was stirred for 4 h at 50 °C. A saturated NH_4Cl solution (3 mL) was added, the layers were separated, and the aqueous layer was extracted with Et_2O (3×5 mL). The combined organic layers were dried (Na_2SO_4), the solvent was removed under

reduced pressure, and the crude product was purified by column chromatography on silica.

Computational Details. The reaction mechanisms of catalytic 1,4-additions to 2-cyclohexenone and 2-cyclopentenone by the complexes [Rh(1)-Ph] and [Rh(2)-Ph] were investigated by density functional theory (DFT) calculations. Minima and transition states were preoptimized using GFN2-xTB,²⁸ optimized on the B3LYP/def2-SVP-D3(BJ) level. The same level was used for the thermal corrections and free-energy contributions at 60 °C. Vibrational frequencies smaller than 100 cm⁻¹ were raised to that value for the thermal analysis to ensure the validity of the RRHO model. On these optimized geometries, energies were calculated at the B2PLYP/def2-TZVP-D3(BJ) level. All DFT calculations were performed in Turbomole V7.1,²⁹ and all geometry optimizations and free-energy calculations were performed in ChemShell³⁰ via DL-FIND.³¹ Of the 16 paths for 1,4-addition to cyclohexenone **6b** with [Rh(1)-Ph] as the catalytic intermediate, the “up” orientation of the C5 atom resulted in the lowest barriers. The “down” orientation of the C5 atom resulted in slightly higher barriers of 70 and 80 kJ/mol for the η^2 -*cis* orientation for (S)- and (R)-products (S)-**8b** and (R)-**8b**, respectively. The barriers resulting from ring binding mode are with 120 and 130 kJ/mol significantly higher. In this case, no transition states for the Si binding mode could be found because of steric hindrance with the ligand, which led to unrealistically high energies. For the phenyl binding mode, the Re approach leads to even higher barriers for Re binding (176 and 189 kJ/mol for “up” and “down”) and to a barrier of 115 kJ/mol for Si binding in the “down” configuration. Si binding in the “up” configuration led to a shift to the respective η^2 -*cis* binding mode.

■ ASSOCIATED CONTENT

Supporting Information

The Supporting Information is available free of charge at <https://pubs.acs.org/doi/10.1021/acs.organomet.0c00310>.

Syntheses, CV, EXAFS, NMR, and crystallographic data (PDF)

Accession Codes

CCDC 1999459–1999460, 1999463, and 1999465 contain the supplementary crystallographic data for this paper. These data can be obtained free of charge via www.ccdc.cam.ac.uk/data_request/cif, or by emailing data_request@ccdc.cam.ac.uk, or by contacting The Cambridge Crystallographic Data Centre, 12 Union Road, Cambridge CB2 1EZ, UK; fax: +44 1223 336033.

■ AUTHOR INFORMATION

Corresponding Authors

Sabine Laschat – *Institut für Organische Chemie, Universität Stuttgart, D-70569 Stuttgart, Germany*; orcid.org/0000-0002-1488-3903; Email: sabine.laschat@oc.uni-stuttgart.de

Thomas Sottmann – *Institut für Physikalische Chemie, Universität Stuttgart, D-70569 Stuttgart, Germany*; orcid.org/0000-0003-3679-3703; Email: thomas.sottmann@ipc.uni-stuttgart.de

Bernd Plietker – *Technische Universität Dresden, Professur für Organische Chemie I, D-01069 Dresden, Germany*; Email: bernd.plietker@tu-dresden.de

Johannes Kästner – *Institut für Theoretische Chemie, Universität Stuttgart, D-70569 Stuttgart, Germany*; orcid.org/0000-0001-6178-7669; Email: johannes.kaestner@theochem.uni-stuttgart.de

Matthias Bauer – *Department Chemie und Center for Sustainable Systems Design (CSSD), Universität Paderborn, D-33098 Paderborn, Germany*; orcid.org/0000-0002-9294-6076; Email: bauerm@mail.uni-paderborn.de

Mark R. Ringenberg – *Institut für Anorganische Chemie, Universität Stuttgart, D-70569 Stuttgart, Germany*; orcid.org/0000-0001-7585-5757; Email: mark.ringenberg@iac.uni-stuttgart.de

Authors

Manuel Kirchhof – *Institut für Organische Chemie, Universität Stuttgart, D-70569 Stuttgart, Germany*

Katrin Gugeler – *Institut für Theoretische Chemie, Universität Stuttgart, D-70569 Stuttgart, Germany*

Felix Richard Fischer – *Institut für Organische Chemie, Universität Stuttgart, D-70569 Stuttgart, Germany*

Michal Nowakowski – *Department Chemie und Center for Sustainable Systems Design (CSSD), Universität Paderborn, D-33098 Paderborn, Germany*

Alina Bauer – *Institut für Organische Chemie, Universität Stuttgart, D-70569 Stuttgart, Germany*

Sonia Alvarez-Barcia – *Institut für Theoretische Chemie, Universität Stuttgart, D-70569 Stuttgart, Germany*; orcid.org/0000-0002-0175-0845

Karina Abitaev – *Institut für Physikalische Chemie, Universität Stuttgart, D-70569 Stuttgart, Germany*

Marc Schnierle – *Institut für Anorganische Chemie, Universität Stuttgart, D-70569 Stuttgart, Germany*

Yaseen Qawasmi – *Institut für Physikalische Chemie, Universität Stuttgart, D-70569 Stuttgart, Germany*

Wolfgang Frey – *Institut für Organische Chemie, Universität Stuttgart, D-70569 Stuttgart, Germany*

Angelika Baro – *Institut für Organische Chemie, Universität Stuttgart, D-70569 Stuttgart, Germany*

Deven P. Estes – *Institut für Technische Chemie, Universität Stuttgart, D-70569 Stuttgart, Germany*; orcid.org/0000-0002-3215-3461

Complete contact information is available at:

<https://pubs.acs.org/doi/10.1021/acs.organomet.0c00310>

Author Contributions

M.K. synthesized ligands and rhodium complexes and carried out the catalysis experiments, K.G. performed DFT calculations, F.R.F. and M.N. performed XAS measurements and EXAFS/XANES analysis, A. Bauer synthesized the enantiomeric ligand and complex, S.A.-B. evaluated the DFT results, K.A. and Y.Q. formulated the microemulsion for the catalysis, M.S. performed CV measurements, W.F. performed all X-ray single crystal structure analyses, A. Baro checked the data and wrote the manuscript, D.P.E. provided his expertise in XAS and proofread the manuscript, T.S. provided his expertise in microemulsions and proofread the manuscript, M.R.R. provided his expertise in metal–organic chemistry and proofread the manuscript, B.P. provided his expertise in metal–organic chemistry and proofread the manuscript, M.B. supervised XAS measurements and XANES/EXAFS analysis and proofread the manuscript, J.K. supervised the DFT calculations as well as wrote and proofread the manuscript, and S.L. coordinated the research as well as wrote and proofread the manuscript.

Notes

The authors declare no competing financial interest.

■ ACKNOWLEDGMENTS

The authors gratefully acknowledge funding by the German Research Foundation (Deutsche Forschungsgemeinschaft, DFG) within the collaborative research center (CRC) 1333,

grant number 358283783, projects A7, B1, B3, C2, C4, S1, the Ministerium für Wissenschaft, Forschung und Kunst des Landes Baden-Württemberg, for generous financial support. M.B. acknowledges funding by the Deutsche Forschungsgemeinschaft (SPP 1708, BA 4467/6-1). The synchrotron PETRA III is kindly acknowledged for beamtime at beamline P65. Part of the infrastructure used for the experiments was realized in the frame of the BMBF projects SynXAS (05K18PPA) and FocusPP64 (05K19PP1). This paper is dedicated to Professor Dr. Wolfgang Kaim on the occasion of his 70th birthday.

REFERENCES

- (1) Hayashi, T.; Ueyama, K.; Tokunaga, N.; Yoshida, K. A Chiral Chelating Diene as a New Type of Chiral Ligand for Transition Metal Catalysts: Its Preparation and Use for the Rhodium-Catalyzed Asymmetric 1,4-Addition. *J. Am. Chem. Soc.* **2003**, *125*, 11508–11509.
- (2) Fischer, C.; Defieber, C.; Suzuki, T.; Carreira, E. M. Readily Available [2.2.2]-Bicyclooctadienes as New Chiral Ligands for Ir(I): Catalytic, Kinetic Resolution of Allyl Carbonates. *J. Am. Chem. Soc.* **2004**, *126*, 1628–1629.
- (3) Maire, P.; Deblon, S.; Breher, F.; Geier, J.; Böhrer, C.; Rügger, H.; Schönberg, H.; Grützmacher, H. Olefins as Steering Ligands for Homogeneously Catalyzed Hydrogenations. *Chem. - Eur. J.* **2004**, *10*, 4198–4205.
- (4) (a) Defieber, C.; Grützmacher, H.; Carreira, E. M. Chiral Olefins as Steering Ligands in Asymmetric Catalysis. *Angew. Chem., Int. Ed.* **2008**, *47*, 4482–4502; *Angew. Chem.* **2008**, *120*, 4558–4579. (b) Johnson, J. B.; Rovis, T. More than Bystanders: The Effect of Olefins on Transition-Metal-Catalyzed Cross-Coupling Reactions. *Angew. Chem., Int. Ed.* **2008**, *47*, 840–871; *Angew. Chem.* **2008**, *120*, 852–884. (c) Maksymowicz, R. M.; Bissette, A. J.; Fletcher, S. P. Asymmetric Conjugate Additions and Allylic Alkylations Using Nucleophiles Generated by Hydro- or Carbometallation. *Chem. - Eur. J.* **2015**, *21*, 5668–5678. (d) Nagamoto, M.; Nishimura, T. Asymmetric Transformations under Iridium/Chiral Diene Catalysis. *ACS Catal.* **2017**, *7*, 833–847.
- (5) (a) Pecchioli, T.; Christmann, M. Synthesis of Highly Enantioenriched Propelladienes and their Application as Ligands in Asymmetric Rh-Catalyzed 1,4-Additions. *Org. Lett.* **2018**, *20*, 5256–5259. (b) Melcher, M.-C.; Rolim Alves da Silva, B.; Ivšić, T.; Strand, D. Chiral Discrimination in Rhodium(I) Catalysis by 2,5-Disubstituted 1,3a,4,6a-Tetrahydropentalene Ligands - More Than Just a Twist of the Olefins? *ACS Omega* **2018**, *3*, 3622–3630. (c) Melcher, M.-C.; Ivšić, T.; Olagnon, C.; Tenten, C.; Lützen, A.; Strand, D. Control of Enantioselectivity in Rhodium(I) Catalysis by Planar Chiral Dibenzocyclooctatetraenes. *Chem. - Eur. J.* **2018**, *24*, 2344–2348. (d) Selmani, A.; Serpier, F.; Darses, S. Chiral Bicyclo[2.2.2]octa-2,5-dienyltrifluoroborate Derivative as a Useful and Stable Precursor of C1-Symmetric Chiral Dienes. *Org. Lett.* **2019**, *21*, 4378–4382. (e) Zhang, B.; Hollerbach, M. R.; Blakey, S. B.; Davies, H. M. L. C-H Functionalization Approach for the Synthesis of Chiral C₂-Symmetric 1,5-Cyclooctadiene Ligands. *Org. Lett.* **2019**, *21*, 9864–9868. (f) Xue, F.; Hayashi, T. Asymmetric Synthesis of Axially Chiral 2-Aminobiaryls by Rhodium-Catalyzed Benzannulation of 1-Arylalkynes with 2-(Cyanomethyl)phenylboronates. *Angew. Chem., Int. Ed.* **2018**, *57*, 10368–10372; *Angew. Chem.* **2018**, *130*, 10525–10529. (g) Li, R.; Wen, Z.; Wu, N. A nordehydroabietyl amide-containing chiral diene for rhodium-catalyzed asymmetric arylation to nitroolefins. *Org. Biomol. Chem.* **2016**, *14*, 11080–11084. (6) (a) Hayashi, T.; Yamasaki, K. Rhodium-Catalyzed Asymmetric 1,4-Addition and Its Related Asymmetric Reactions. *Chem. Rev.* **2003**, *103*, 2829–2844. (b) Yasukawa, T.; Kuremoto, T.; Miyamura, H.; Kobayashi, S. Asymmetric Arylation of Imines Catalyzed by Heterogeneous Chiral Rhodium Nanoparticles. *Org. Lett.* **2016**, *18*, 2716–2718. (c) Chen, C. C.; Gopula, B.; Syu, J.-F.; Pan, J.-H.; Kuo, T.-S.; Wu, P.-Y.; Henschke, J. P.; Wu, H.-L. Enantioselective and Rapid Rh-Catalyzed Arylation of *N*-Tosyl- and *N*-Nosylaldimines in Methanol. *J. Org. Chem.* **2014**, *79*, 8077–8085. (d) Dou, X.; Lu, Y.; Hayashi, T. Base-Free Conditions for Rhodium-Catalyzed Asymmetric Arylation To Produce Stereochemically Labile α -Aryl Ketones. *Angew. Chem., Int. Ed.* **2016**, *55*, 6739–6743; *Angew. Chem.* **2016**, *128*, 6851–6855. (e) Zhou, B.; Ming So, C.; Lu, Y.; Hayashi, T. A chiral bicyclo[2.2.2]octa-2,5-diene ligand substituted with the ferrocenyl group and its use for rhodium-catalyzed asymmetric 1,4-addition-reactions. *Org. Chem. Front.* **2015**, *2*, 127–132. (f) Luo, Y.; Hepburn, H. B.; Chotsaeng, N.; Lam, H. W. Enantioselective Rhodium-Catalyzed Nucleophilic Allylation of Cyclic Imines with Allylboron Reagents. *Angew. Chem., Int. Ed.* **2012**, *51*, 8309–8313; *Angew. Chem.* **2012**, *124*, 8434–8438. (g) Nishimura, T.; Nagai, T.; Takechi, R.; Ebe, Y. Rhodium-Catalyzed Enantioselective Addition of Tricyclopropylboroxin to *N*-Sulfonylimines. *Synthesis* **2016**, *48*, 2612–2618. (h) Choi, K.; Park, H.; Lee, C. Rhodium-Catalyzed Tandem Addition-Cyclization-Rearrangement of Alkynylhydrazones with Organoboronic Acids. *J. Am. Chem. Soc.* **2018**, *140*, 10407–10411. (i) Xue, F.; Liu, Q.; Zhu, Y.; Qing, Y.; Wan, B. Chiral benzene backbone-based sulfoxide-olefin ligands for highly enantioselective Rh-catalyzed addition of arylboronic acids to *N*-tosylarylimines. *RSC Adv.* **2019**, *9*, 25377–25381. (j) Moku, B.; Fang, W.; Leng, J.; Kantchev, E. A. B.; Qin, H. Rh(I)-Diene-Catalyzed Addition of (Hetero)aryl Functionality to 1,3-Dienylsulfanyl Fluorides Achieving Exclusive Regioselectivity and High Enantioselectivity: Generality and Mechanism. *ACS Catal.* **2019**, *9*, 10477–10488. (k) Moku, B.; Fang, W.; Leng, J.; Li, L.; Zha, G.; Rakesh, K. P.; Qin, H. Rh-Catalyzed Highly Enantioselective Synthesis of Aliphatic Sulfanyl Fluorides. *iScience* **2019**, *21*, 695–705. (7) (a) Aikawa, K.; Takabayashi, Y.; Kawachi, S.; Mikami, K. Axial chirality control of tropisBIPHEP-Rh complexes by chiral dienes: synergy effect in catalytic asymmetric hydrogenation. *Chem. Commun.* **2008**, 5095–5097. (b) Liu, Y.; Du, H. Chiral Dienes as “Ligands” for Borane-Catalyzed Metal-Free Asymmetric Hydrogenation of Imines. *J. Am. Chem. Soc.* **2013**, *135*, 6810–6813. (c) Punniyamurthy, T.; Mayr, M.; Dorofeev, A. S.; Bataille, C. J. R.; Gosiewska, S.; Nguyen, B.; Cowley, A. R.; Brown, J. M. Enantiomerically pure bicyclo[3.3.1]nona-2,6-diene as the sole source of enantioselectivity in BIPHEP-Rh asymmetric hydrogenation. *Chem. Commun.* **2008**, 5092–5094. (8) (a) Hatano, M.; Nishimura, T. Hydroxo-iridium/Chiral Diene Complexes as Effective Catalysts for Asymmetric Annulation of *t*-Oxo- and Iminocarboxamides with 1,3-Dienes. *Angew. Chem., Int. Ed.* **2015**, *54*, 10949–10952; *Angew. Chem.* **2015**, *127*, 11099–11102. (b) Nishimura, T.; Yasuhara, Y.; Hayashi, T. Iridium-Catalyzed [3 + 2] Annulation of 1,3-Dienes with ortho-Carbonylated Phenylboronic Acids. A Catalytic Process Involving Regioselective 1,2-Addition. *J. Am. Chem. Soc.* **2007**, *129*, 7506–7507. (c) Shintani, R.; Sannohe, Y.; Tsuji, T.; Hayashi, T. A Cationic Rhodium-Chiral Diene Complex as a High-Performance Catalyst for the Intramolecular Asymmetric [4 + 2] Cycloaddition of Alkyne-1,3-Dienes. *Angew. Chem., Int. Ed.* **2007**, *46*, 7277–7280; *Angew. Chem.* **2007**, *119*, 7415–7418. (9) (a) Baudry, D.; Ephritikhine, M.; Felkin, H. Isomerisation of allyl ethers catalysed by the cationic iridium complex [Ir(cyclo-octa-1,5-diene)(PMePh₂)₂]PF₆. A highly stereoselective route to trans-propenyl ethers. *J. Chem. Soc., Chem. Commun.* **1978**, 694–695. (b) Nishimura, T.; Katoh, T.; Takatsu, K.; Shintani, R.; Hayashi, T. Rhodium-Catalyzed Asymmetric Rearrangement of Alkynyl Alkenyl Carbinols: Synthetic Equivalent to Asymmetric Conjugate Alkynylation of Enones. *J. Am. Chem. Soc.* **2007**, *129*, 14158–14159. (c) Nishimura, T.; Kawamoto, T.; Nagaosa, M.; Kumamoto, H.; Hayashi, T. Chiral Tetrafluorobenzobarrelene Ligands for the Rhodium-Catalyzed Asymmetric Cycloisomerization of Oxygen- and Nitrogen-Bridged 1,6-Enynes. *Angew. Chem., Int. Ed.* **2010**, *49*, 1638–1641; *Angew. Chem.* **2010**, *122*, 1682–1685. (10) Chen, D.; Zhang, X.; Qi, W.-Y.; Xu, B.; Xu, M.-H. Rhodium(I)-Catalyzed Asymmetric Carbene Insertion into B-H Bonds: Highly Enantioselective Access to Functionalized Organoboranes. *J. Am. Chem. Soc.* **2015**, *137*, 5268–5271. (11) (a) Chen, D.; Zhu, D.-X.; Xu, M.-H. Rhodium(I)-Catalyzed Highly Enantioselective Insertion of Carbenoid into Si-H: Efficient Access to Functional Chiral Silanes. *J. Am. Chem. Soc.* **2016**, *138*, 1498–1501. (b) Ichikawa, Y.; Nishimura, T.; Hayashi, T. Rhodium/Chiral

- Diene-Catalyzed Asymmetric Cyclopolymerization of Achiral 1,8-Diynes. *Organometallics* **2011**, *30*, 2342–2348. (c) Johnson, T.; Choo, K.-L.; Lautens, M. Rhodium-Catalyzed Arylative Cyclization for the Enantioselective Synthesis of (Trifluoromethyl)cyclobutanols. *Chem. - Eur. J.* **2014**, *20*, 14194–14197. (d) Ma, X.; Jiang, J.; Lv, S.; Yao, W.; Yang, Y.; Liu, S.; Xia, F.; Hu, W. An Ylide Transformation of Rhodium(I) Carbene: Enantioselective Three-Component Reaction through Trapping of Rhodium(I)-Associated Ammonium Ylides by β -Nitroacrylates. *Angew. Chem., Int. Ed.* **2014**, *53*, 13136–13139; *Angew. Chem.* **2014**, *126*, 13352–13355. (e) Nishimura, T.; Ichikawa, Y.; Hayashi, T.; Onishi, N.; Shiotsuki, M.; Masuda, T. Asymmetric Polymerization of Achiral Arylacetylenes Giving Helical Polyacetylenes in the Presence of a Rhodium Catalyst with a C_2 -Symmetric Tetrafluorobenzobarrelene Ligand. *Organometallics* **2009**, *28*, 4890–4893. (f) Nishimura, T.; Maeda, Y.; Hayashi, T. Asymmetric Cyclopropanation of Alkenes with Dimethyl Diazomalonate Catalyzed by Chiral Diene-Rhodium Complexes. *Angew. Chem., Int. Ed.* **2010**, *49*, 7324–7327; *Angew. Chem.* **2010**, *122*, 7482–7485. (g) Nishimura, T.; Noishiki, A.; Hayashi, T. Electronic tuning of chiral diene ligands in iridium-catalyzed asymmetric 1,6-addition of arylboroxines to δ -aryl- $\alpha,\beta,\gamma,\delta$ -unsaturated ketones. *Chem. Commun.* **2012**, *48*, 973–975. (h) Nishimura, T.; Takiguchi, Y.; Maeda, Y.; Hayashi, T. Rhodium-Catalyzed Asymmetric Cycloisomerization of 1,6-Ene-ynamides. *Adv. Synth. Catal.* **2013**, *355*, 1374–1382. (i) Nishimura, T.; Yasuhara, Y.; Sawano, T.; Hayashi, T. Iridium-Catalyzed Enantioselective 1,6-Addition. *J. Am. Chem. Soc.* **2010**, *132*, 7872–7873. (j) Serpier, F.; Flamme, B.; Brayer, J.-L.; Folléas, B.; Darses, S. Chiral Pyrrolidines and Piperidines from Enantioselective Rhodium-Catalyzed Cascade Arylative Cyclization. *Org. Lett.* **2015**, *17*, 1720–1723. (k) Shibata, T.; Shizuno, T. Iridium-Catalyzed Enantioselective C-H Alkylation of Ferrocenes with Alkenes Using Chiral Diene Ligands. *Angew. Chem., Int. Ed.* **2014**, *53*, 5410–5413; *Angew. Chem.* **2014**, *126*, 5514–5517. (l) Shintani, R.; Okamoto, K.; Otomaru, Y.; Ueyama, K.; Hayashi, T. Catalytic Asymmetric Arylative Cyclization of Alkynals: Phosphine-Free Rhodium/Diene Complexes as Efficient Catalysts. *J. Am. Chem. Soc.* **2005**, *127*, 54–55. (m) Zhang, S.-S.; Wang, Z.-Q.; Xu, M.-H.; Lin, G.-Q. Chiral Diene as the Ligand for the Synthesis of Axially Chiral Compounds via Palladium-Catalyzed Suzuki-Miyaura Coupling Reaction. *Org. Lett.* **2010**, *12*, 5546–5549.
- (12) Zhang, P.; Wang, H.; Shi, X.; Yan, X.; Wu, X.; Zhang, S.; Yao, B.; Feng, X.; Zhi, J.; Li, X.; Tong, B.; Shi, J.; Wang, L.; Dong, Y. On-Water Polymerization of Phenylacetylene Catalyzed by Rh Complexes Bearing Strong π -Acidic Dibenzo[a, e]cyclooctatetraene Ligand. *J. Polym. Sci., Part A: Polym. Chem.* **2017**, *55*, 716–725.
- (13) Lipshutz, B. H.; Isley, N. A.; Moser, R.; Ghorai, S.; Leuser, H.; Taft, B. R. Rhodium-Catalyzed Asymmetric 1,4-Additions, in Water at Room Temperature, with In-Flask Catalyst Recycling. *Adv. Synth. Catal.* **2012**, *354*, 3175–3179.
- (14) Haag, D.; Runsink, J.; Scharf, H.-D. [L^* Rh(NBD)Cl] (L^* = Chiral Cyclic Monophosphonite): A Novel Class of Rhodium(I) Complexes and Their Evaluation in the Asymmetric Hydrosilylation of Ketones. Investigations of the Effects of Temperature and Ligand Backbone. *Organometallics* **1998**, *17*, 398–409.
- (15) (a) Nishimura, T.; Kumamoto, H.; Nagaosa, M.; Hayashi, T. The concise synthesis of chiral tfb ligands and their application to the rhodium-catalyzed asymmetric arylation of aldehydes. *Chem. Commun.* **2009**, 5713–5715. (b) Shintani, R.; Soh, Y.-T.; Hayashi, T. Rhodium-Catalyzed Asymmetric Arylation of Azomethine Imines. *Org. Lett.* **2010**, *12*, 4106–4109.
- (16) Kina, A.; Ueyama, K.; Hayashi, T. Enantiomerically Pure Rhodium Complexes Bearing 1,5-Diphenyl-1,5-cyclooctadiene as a Chiral Diene Ligand. Their Use as Catalysts for Asymmetric 1,4-Addition of Phenylzinc Chloride. *Org. Lett.* **2005**, *7*, 5889–5892.
- (17) Nishimura, T.; Maeda, Y.; Hayashi, T. Chiral Diene-Phosphine Tridentate Ligands for Rhodium-Catalyzed Asymmetric Cycloisomerization of 1,6-Enynes. *Org. Lett.* **2011**, *13*, 3674–3677.
- (18) (a) Pollice, R.; Schnürch, M. Expansion of the Concept of Nonlinear Effects in Catalytic Reactions Beyond Asymmetric Catalysis. *Chem. - Eur. J.* **2016**, *22*, 5637–5642. (b) Duan, W.-L.; Iwamura, H.; Shintani, R.; Hayashi, T. Chiral Phosphine-Olefin Ligands in the Rhodium-Catalyzed Asymmetric 1,4-Addition Reactions. *J. Am. Chem. Soc.* **2007**, *129*, 2130–2138.
- (19) (a) Chen, D.; Zhu, D.-X.; Xu, M.-H. Rhodium(I)-Catalyzed Highly Enantioselective Insertion of Carbenoid into Si-H: Efficient Access to Functional Chiral Silanes. *J. Am. Chem. Soc.* **2016**, *138*, 1498–1501. (b) Itooka, R.; Iguchi, Y.; Miyaura, N. Rhodium-Catalyzed 1,4-Addition of Arylboronic Acids to α,β -Unsaturated Carbonyl Compounds: Large Accelerating Effects of Bases and Ligands. *J. Org. Chem.* **2003**, *68*, 6000–6004.
- (20) (a) Zhang, L.; Tan, M.; Zhou, L.; Zeng, Q. A novel, C_2 -symmetric, chiral bis-cyclohexylamine-olefin tridentate ligand in Rh-catalyzed asymmetric 1,4-additions. *Tetrahedron Lett.* **2018**, *59*, 2778–2783. (b) Yasukawa, T.; Miyamura, H.; Kobayashi, S. Cellulose-supported chiral rhodium nanoparticles as sustainable heterogeneous catalysts for asymmetric carbon-carbon bond-forming reactions. *Chem. Sci.* **2015**, *6*, 6224–6229. (c) Ogasawara, M.; Tseng, Y.-Y.; Arae, S.; Morita, T.; Nakaya, T.; Wu, W.-Y.; Takahashi, T.; Kamikawa, K. Phosphine-Olefin Ligands Based on a Planar-Chiral (π -Arene)-chromium Scaffold: Design, Synthesis, and Application in Asymmetric Catalysis. *J. Am. Chem. Soc.* **2014**, *136*, 9377–9384. (d) Vlahovic, S.; Schädel, N.; Tussetschläger, S.; Laschat, S. Tropanes as Scaffolds for Phosphorus-Olefin Ligands and Their Application in Asymmetric Catalysis. *Eur. J. Org. Chem.* **2013**, 1580–1590. (e) Gendrineau, T.; Genet, J.-P.; Darses, S. Room-Temperature Rhodium-Catalyzed Asymmetric 1,4-Addition of Potassium Trifluoro(organo)borates. *Org. Lett.* **2009**, *11*, 3486–3489. (f) Otomaru, Y.; Kina, A.; Shintani, R.; Hayashi, T. C_2 -Symmetric bicyclo[3.3.1]nona-2,6-diene and bicyclo[3.3.2]deca-2,6-diene: new chiral diene ligands based on the 1,5-cyclooctadiene framework. *Tetrahedron: Asymmetry* **2005**, *16*, 1673–1679.
- (21) (a) Mühlhäuser, T.; Savin, A.; Frey, W.; Baro, A.; Schneider, A. J.; Döteberg, H.-G.; Bauer, F.; Köhn, A.; Laschat, S. Role of Regioisomeric Bicyclo[3.3.0]octa-2,5-diene Ligands in Rh Catalysis: Synthesis, Structural Analysis, Theoretical Study, and Application in Asymmetric 1,2- and 1,4-Additions. *J. Org. Chem.* **2017**, *82*, 13468–13480. (b) Gosiewska, S.; Raskatov, J. A.; Shintani, R.; Hayashi, T.; Brown, J. M. The Origins of Enantioselectivity in Rh-Diene Complex Catalyzed Arylation of Cyclohex-2-enones. *Chem. - Eur. J.* **2012**, *18*, 80–84. (c) Hayashi, T.; Takahashi, M.; Takaya, Y.; Ogasawara, M. Catalytic Cycle of Rhodium-Catalyzed Asymmetric 1,4-Addition of Organoboronic Acids. Arylrhodium, Oxa- π -allylrhodium, and Hydroxorhodium Intermediates. *J. Am. Chem. Soc.* **2002**, *124*, 5052–5058. (d) Kantchev, E. A. B. The origin of regio- and enantioselectivity in the Rh/chiral 1,4-diene-catalyzed addition of phenylboronic acid to enones: insights from DFT. *Chem. Commun.* **2011**, 47, 10969–10971. (e) Kantchev, E. A. B. Cooperativity between steric repulsion and crossed diene coordination governs the enantioselectivity in rhodium-(I)/chiral, 1,4- and 1,5-diene-catalyzed 1,4-addition reaction: a DFT study. *Chem. Sci.* **2013**, *4*, 1864–1875. (f) Qin, H.-L.; Chen, X.-Q.; Shang, Z.-P.; Kantchev, E. A. B. The Challenge of Linear (E)-Enones in the Rh-Catalyzed, Asymmetric 1,4-Addition Reaction of Phenylboronic Acid: A DFT Computational Analysis. *Chem. - Eur. J.* **2015**, *21*, 3079–3086.
- (22) Deimling, M.; Kirchhof, M.; Schwager, B.; Qawasm, Y.; Savin, A.; Mühlhäuser, T.; Frey, W.; Claasen, B.; Baro, A.; Sottmann, T.; Laschat, S. Asymmetric Catalysis in Liquid Confinement: Probing the Performance of Novel Chiral Rhodium-Diene Complexes in Microemulsions and Conventional Solvents. *Chem. - Eur. J.* **2019**, *25*, 9464–9476.
- (23) Spek, A. L. PLATON SQUEEZE: a tool for the calculation of the disordered solvent contribution to the calculated structure factors. *Acta Crystallogr., Sect. C: Struct. Chem.* **2015**, *71*, 9–18.
- (24) Sieffert, N.; Boisson, J.; Py, S. Enantioselective Arylation of N-Tosylimines by Phenylboronic Acid Catalyzed by a Rhodium/Diene Complex: Reaction Mechanism from Density Functional Theory. *Chem. - Eur. J.* **2015**, *21*, 9753–9768.

(25) Desnoyer, A. N.; Behyan, S.; Patrick, B. O.; Dauth, A.; Love, J. A.; Kennepohl, P. Reexamining Oxidation States during the Synthesis of 2-Rhodoxetanes from Olefins. *Inorg. Chem.* **2016**, *55*, 13–15.

(26) Lauterwasser, F.; Vanderheiden, S.; Bräse, S. Planar- and Central-Chiral *N,O*-[2.2]Paracyclophane Ligands: Non-Linear-Like Effects and Activity. *Adv. Synth. Catal.* **2006**, *348*, 443–448.

(27) Chahdoura, F.; Dubrulle, L.; Fourmy, K.; Durand, J.; Madec, D.; Gomez, M. Glycerol - A Non-Innocent Solvent for Rh-Catalysed Pauson-Khand Carbocyclisations. *Eur. J. Inorg. Chem.* **2013**, *2013*, 5138–5144.

(28) Bannwarth, C.; Ehlert, S.; Grimme, S. GFN2-xTB - An Accurate and Broadly Parametrized Self-Consistent Tight-Binding Quantum Chemical Method with Multipole Electrostatics and Density-Dependent Dispersion Contributions. *J. Chem. Theory Comput.* **2019**, *15*, 1652–1671.

(29) TURBOMOLE V7.1 2016, a development of University of Karlsruhe and Forschungszentrum Karlsruhe GmbH, 1989–2007, TURBOMOLE GmbH, since 2007.

(30) (a) Sherwood, P.; de Vries, A. H.; Guest, M. F.; Schreckenbach, G.; Catlow, C. R. A.; French, S. A.; Sokol, A. A.; Bromley, S. T.; Thiel, W.; Turner, A. J.; Billeter, S.; Terstegen, F.; Thiel, S.; Kendrick, J.; Rogers, S. C.; Casci, J.; Watson, M.; King, F.; Karlsen, E.; Sjøvoll, M.; Fahmi, A.; Schäfer, A.; Lennartz, C. QUASI: A general purpose implementation of the QM/MM approach and its application to problems in catalysis. *J. Mol. Struct.: THEOCHEM* **2003**, *632*, 1–28. (b) Metz, S.; Kästner, J.; Sokol, A. A.; Keal, T. W.; Sherwood, P. ChemShell - a modular software package for QM/MM simulations. *Wiley Interdiscip. Rev.: Comput. Mol. Sci.* **2014**, *4*, 101–110.

(31) Kästner, J.; Carr, J. M.; Keal, T. W.; Thiel, W.; Wander, A.; Sherwood, P. DL-FIND: An Open-Source Geometry Optimizer for Atomistic Simulations. *J. Phys. Chem. A* **2009**, *113*, 11856–11865.